به نام خدا

مرکز دانلود رایگان
مهندسی متالورژی و مواد

ENN Encyclopedia of Nanoscience and Nanotechnology
www.aspbs.com/enn

Nanocrystalline Ceramics by Mechanical Activation

J. M. Xue, Z. H. Zhou, J. Wang

National University of Singapore, Singapore

CONTENTS

1. Introduction
2. Mechanically Activated Processes
3. Mechanical Activation Devices
4. Nanocrystalline Ceramic Materials
5. Nanocrystalline Ceramics by Mechanical Activation
6. Mechanical Crystallization and Precursor to Ceramic Conversions
7. Summary
Glossary
References

1. INTRODUCTION

Ceramic materials are traditionally synthesized by solid-state reactions of the starting constituents (such as oxides, nonoxides, carbonates, and precursors) at elevated temperatures. It is, however, difficult to realize a nanocrystalline feature by the conventional ceramic process, as a high temperature calcination always leads to coarsening and aggregation of fine ceramic particles. Similarly, most of the wet-chemistry-based processing routes for ceramic materials have failed to deliver a true nanocrystalline structure, again due to the unwanted particle and crystallite coarsening and aggregation at the calcination temperature, which is unavoidably required for chemistry-derived ceramic precursors. In a fundamentally different approach, phase formation in mechanical activation is realized at room temperature, via one or more of the mechanically triggered chemical reactions, nucleation and growth from an amorphous state, decompositions, and phase transformations, depending on the specific ceramic material concerned. Little progress was made in synthesizing ceramic materials by mechanical activation until about 10 years ago when the potential of this novel synthesis technique was demonstrated, although mechanical alloying for metals and intermetallics was devised more than 30 years ago. Over the past 5 years, there has been a surge in effort to employ mechanical activation for synthesis of a wide range of nanocrystalline ceramic materials including ceramic oxides, oxides of complex perovskite, spinel and layer structures, nonoxides, magnetic ceramics, electroceramics, and ceramic nanocomposites. While research focus on mechanical activation, on the one hand, is directed at synthesis of nanocrystalline ceramic materials, many of the underlying physical phenomena in association with mechanical activation have yet to be properly studied and made understood. On the other hand, mechanical activation promises a significant technological implication, whereby the currently employed multiple steps of phase-forming calcination/annealing at high temperatures for ceramic materials can be skipped, when the required nanocrystalline ceramic phases are realized at room temperature in an enclosed mechanical activation chamber. In this chapter, recent progress in mechanical activation for synthesis of nanocrystalline ceramic materials is reviewed and a number of new and unique phenomena brought about by mechanical activation in functional ceramics are discussed, together with a short discussion on the possible future development of this novel technique.

2. MECHANICALLY ACTIVATED PROCESSES

Mechanically activated processes are among the earliest phenomena created by humankind and the use of flint to trigger fires is perhaps one of the best known examples [1]. Mechanochemical reactions were documented and date back as early as several hundred B.C., when a number of chemical reactions were noted under the influence of one or more types of mechanical actions. However, mechanochemistry was not developed in a systematic manner until late 19th century, along with solid state chemistry, when the

ISBN: 1-58883-062-4/$35.00
Copyright © 2004 by American Scientific Publishers
All rights of reproduction in any form reserved.

Encyclopedia of Nanoscience and Nanotechnology
Edited by H. S. Nalwa
Volume 6: Pages (417–433)

effects of high pressure, mechanical impact, and combination of high pressure and temperature on the rates of solid state chemical reactions and phase transitions were studied [2]. Following the steady establishment of physical metallurgy in the first half of 20th century and then materials science, the potential of mechanically activated processes for materials synthesis was first demonstrated by Benjamin [3], who devised "mechanically alloying" for oxide-dispersed nickel- and iron-based super alloys. This marked a new era of successfully employing mechanically activated process in materials synthesis, and it was followed by the extension and application of this novel technique to a wide range of structural and functional materials, including intermetallics and metal matrix composites in the early stage of development, and then magnetic materials, semiconductors, and more recently nanocrystalline ceramic materials and ceramic matrix composites.

In the recent development history of mechanically activated processes, there existed a number of terminologies, each of which was adopted by the inventor of a specific fabrication technique [4]. In several cases, there is no clear boundary between two or more such terminologies. Mechanical alloying is used to describe a process where the powder mixture of different metals, alloys, or compounds is ultimately mixed together and the formation of a new alloy phase involves mass transfer. In comparison, mechanical milling refers to a milling process of homogenized compositions where mass transfer is not required. Therefore, it is often associated with milling of a pure metal or compound that is already in a state of thermodynamic equilibrium. Similarly, mechanical grinding refers to a milling process where mechanical milling is dominated by abrasion or shear stresses and chip formation. Mechanical disordering is specifically phrased for the milling process that is designed for destruction of the long-range order in intermetallics and production of either a disordered intermetallic or an amorphous phase. Mechanical crystallization describes the nucleation and crystallite growth triggered by a mechanical process from either an amorphous state or an amorphous precursor.

Mechanochemical synthesis/process is the general phrase that has been widely given to any high energy milling process of powdered materials involving one or more chemical reactions occurring during milling [5, 6]. Most of the mechanically activated processes for synthesis of nanocrystalline ceramic materials fall into this category. In mechanochemical synthesis, mechanical activation is employed to trigger the chemical reaction, structural change, and nucleation and growth of nanocrystallites from an amorphous state, leading to a product phase, with or without the need of a further thermal treatment at elevated temperatures. In combination with mechanical alloying, mechanochemical synthesis has been used to describe majority of the mechanically activated processes that have been devised and utilized in materials synthesis, while several other terms, such as reactive milling [7], rod milling [8], and mechanically activated self-propagating high temperature synthesis [9], can easily be categorized into either of these two general categories. Reaction milling, for example, pertains to the mechanical alloying process that is accompanied by one or more solid state reactions. Rod milling is a specific technique that was developed in Japan to trigger the mechanochemical reaction by a predominant shear process, in order to reduce the level of contamination. Mechanically activated self-propagating high temperature synthesis refers to any mechanically activated reaction that is self-propagating in nature once triggered [10], which again can be categorized into the general terminology of mechanochemical synthesis. It must be pointed out that phase formation of several nanocrystalline ceramic materials, such as those via nucleation and subsequent crystallite growth from an amorphous state, is not a result of any chemical reactions that are described in the traditional mechanochemical process. Therefore, the terminology of mechanical activation is adopted in this chapter, which is aimed at covering most of the mechanically activated processes for synthesis of nanocrystalline ceramic materials.

3. MECHANICAL ACTIVATION DEVICES

Although syntheses of ceramic materials and many other types of materials have been successfully realized by various mechanically activated processes, there has been little specification and standardization with the types of mechanical activation devices and setups [4]. Conventional ball milling, which is commonly employed for mixing and blending of raw materials and refinement in particle and agglomerate sizes in ceramic industry, is generally unsuitable for mechanochemical synthesis, although certain phase transformations (such as those in PbO) and a number of chemical reactions can occur in conventional ball milling. Generally speaking, mechanical activation devices are those of high energy milling and modifications of high energy milling, which were originally designed for mechanical alloying. SPEX shaker mills and planetary ball mills are among the very few choices of commercially available high energy mills. SPEX Shaker mills are designed for a relatively small capacity of up to 20 grams and are therefore popularly adopted for laboratory investigation. They typically consist of one vial, containing the sample composition and activation media (typically of one or more high density balls made of ceramics or stainless steel), secured in clamps and swung energetically back and forth up to several thousand times per minute. The back and forth shaking motion of the vial is also combined with lateral movements. By simple calculation, ball velocity in SPEX Shaker mills is up to the order of 5 m/s, generating an unusually high impact force at a very high frequency.

Planetary mills, which are designed for relatively large quantities in the range up to a few hundred grams of powder per batch, are manufactured by Fritsch GmbH in Germany. Vials of planetary mills are arranged on a rotating support disk by a specifically designed drive mechanism to cause them to rotate around their own axes. There is a strong centrifugal force produced by the rotating vials around their own axes, together with that generated by the rotating support disk; both act on the vial contents and the activation balls. Because the vials and the supporting disk rotate in opposite directions, the centrifugal forces alternately act in like and opposite directions. This enables the activation balls to run against the internal walls of the vial, generating a friction effect, and at the same time the activation balls lift off and travel freely through the inner chamber of the vial and collide against the opposing inside wall generating a strong impact effect.

An attrition mill, which is a modification of the conventional ball mill, consists of a vertically aligned drum with several impellers being set progressively at right angles to each other. The impellers energize the medium charge, causing impacts between activation media, between the medium and the drum wall, and between the medium, agitator shaft, and impeller. Attrition mills are capable of larger batch quantity (up to tens of kilos) than both planetary mills and shaker mills, although they are generally regarded as being of low energy type and unsuitable for successful mechanical activation syntheses in many cases.

There have been several new designs of mechanical activation devices, including rod mills, vibrating mills, and those shaker and planetary mills in combination with the application of an electrical discharge, magnetic field, temperature, and hydrothermal conditions, in an effort to combine mechanical activation with other processing controls [11–14]. Typical processing parameters that can be controlled in mechanical activation include the activation (or mill) speed, activation time, choices, size and combination of vial and milling media, media to powder weight ratio, activation media and atmosphere, activation temperature, and pressure.

4. NANOCRYSTALLINE CERAMIC MATERIALS

Performance and functional properties of ceramic materials are critically dependent on a number of compositional and structural parameters in atomic, nanometer, and microstructural scales. Over the past four decades starting from the 1960s following the wide application of electron microscopes in materials characterization, there has been a steady accumulation of knowledge and understanding on the microstructure and microstructure–property relationships in ceramic materials. At the same time, in particular over the past two decades, research focus on ceramic processing has been shifting from the traditional solid state reactions to wet-chemistry-based syntheses, in order to refine the microstructure into nanometer scales. There are two major driving forces behind the current surge in pursuit of a nanocrystalline structure for ceramic materials: (i) the unique physical and functional properties arising from a nanostructure and (ii) a much lowered processing temperature for ceramic materials.

As a result of the significant refinement in particle size (for powdered ceramics) and grain size (for sintered bulk ceramics) into the nanometer range, surfaces, interfaces, and grain boundaries play a critically important role in determining the physical and functional behaviors of nanocrystalline and nanostructured ceramic materials, which can be considerably different from those of their counterparts with structural features in the micrometer scales. For example, a flexural strength of >2000 MPa and excellent superplasticity, which were traditionally considered as being impossible for brittle ceramic materials, have been demonstrated with both oxide ceramics (alumina and zirconia) and ceramic nanocomposites (e.g., alumina–SiC and Si_3N_4–SiC) [15–17].

Ultrafine ceramic powders consisting of well dispersed nanocrystalline particles of <100 nm in size have received considerable attention for technologically demanding application in micro- and nanoelectronics, materials processing and manufacturing, medicine and biotechnology, catalysts, new energy sources, and environmental protections. As a result of the much enlarged surface to volume ratio and one or more quantum and confinement effects, nanocrystalline ceramic particles exhibit many unique properties that can be fundamentally different from those of their coarse counterparts. Nanocrystalline ferrites of spinel structure are among many such well established examples. For example, zinc ferrite ($ZnFe_2O_4$) in bulk ceramic form possesses a normal spinel structure with the tetrahedral A sites exclusively being occupied by Zn^{2+} ions. As such, the predominant magnetic interaction in $ZnFe_2O_4$ is the weak B–B interaction (i.e., the negative superexchange interaction among Fe^{3+} ions in the octahedral sites) [18, 19]. $ZnFe_2O_4$ is therefore traditionally regarded as an antiferromagnetic with Néel temperature of about 10 K, above which it becomes paramagnetic. Several unusual magnetic phenomena have been observed in nanosized zinc ferrite particles synthesized via a number of different processing routes, including mechanical activation [20–24]. They exhibit unusually high magnetizations and higher Néel temperatures than those of bulk $ZnFe_2O_4$. Recent investigation has confirmed that this is related to a partially inverted spinel structure in the nanocrystalline $ZnFe_2O_4$ particles, in which a small number of Fe^{3+} ions occupy the tetrahedral A sites, causing formation of magnetic clusters by the A–B interactions [25]. A similar structure disorder has been observed in nanocrystalline $NiFe_2O_4$ derived from mechanical activation [26].

Employment of nanocrystalline ceramic powders as the starting materials can dramatically lower the sintering temperature of ceramic materials. While many ceramic materials are indispensable for functioning of almost all electronic, microelectronic, and data storage devices, integration of ceramic materials into wafer-based technology inevitably requires a processing temperature for ceramic materials be compatible to those for silicon and wafer technology. There is therefore a significant technological implication in lowering the sintering temperature of these ceramic materials. For example, use of an electroceramic material in co-fired mulitlayer devices requires the electroceramic composition be sinterable at a temperature below 1000 °C. A low enough firing temperature will apparently alleviate, if not completely eliminate, the detrimental interactions between alternative layers of ceramic and metal electrode at the co-firing temperature. For multilayer ceramic capacitors, for example, a large enough reduction in sintering temperature will lead to substitution of the very expensive electrodes of platinum and palladium, by much cheaper ones, such as those made of silver, nickel, copper, and their alloys [27].

To prepare nanocrystalline ceramic particles, many chemistry-based processing routes have been attempted, including for example, sol–gel [28], hydrolysis [29], hydrothermal reaction [30], and coprecipitation [31]. Chemistry-based processing techniques inevitably use high-purity inorganic, organic, and metallorganic chemicals as the starting materials, and they are associated with high production cost and low production yield. Furthermore, almost all the chemistry-derived precursors require a calcination step at elevated temperatures, which unfortunately ruins almost all the advantages offered by chemistry-based novel processing techniques, including a very high specific surface area, ultrafine particle size, and narrow particle size distribution. Any thermal annealing and calcination inevitably causes crystallite coarsening and particle aggregation in the resulting ceramic powders. The occurrence of hard particle aggregates adversely affects subsequent compaction and sintering behaviors and leads to a low density and the occurrence of microstructural defects in sintered ceramic bodies. In the ceramic industry, one or more postcalcination conventional ball milling steps are often carried out, in order to modify the particle characteristics (e.g., particle and aggregate sizes, particle morphology) before subsequent shaping and then sintering at high temperatures. However, hard enough particle aggregates cannot be effectively eliminated by a conventional ball mill.

In a fundamentally different approach from the conventional ceramic processing and most chemistry-based synthesis techniques for ceramic materials, mechanical activation offers the following distinctions and advantages:

(i) In mechanical activation, phase formation is realized by an input of mechanical activation, instead of the thermal activation (i.e., calcination and annealing at high temperatures) that is employed in the conventional ceramic processing and most chemistry-based synthesis routes.

(ii) Mechanical activation is conducted at a much lower temperature, often at room temperature, than required in either conventional ceramic processing or wet-chemistry-based synthesis routes.

(iii) Ceramic phases derived from mechanical activation exhibit a nanocrystallinity and particle sizes in the nanometer range, together with a minimized degree of particle agglomeration.

(iv) Being conducted in an enclosed chamber and by skipping the thermal activation at elevated temperatures for phase formation, mechanical activation exercises a strict control on chemical and compositional stoichiometry, which is critically important for functional and electroceramic materials where volatile components are often lost at the solid state reaction or calcination temperatures.

(v) Mechanical activation employs commonly available ceramic raw materials, such as oxides and nonoxides as the starting materials, and at the same time skips the phase-formation calcination and postcalcination communition, leading to a much lower production cost than that of either conventional ceramic processing or a chemistry-based synthesis route.

(vi) Nanocrystalline ceramic materials derived from mechanical activation demonstrate a number of unique structural and physical behaviors, such as structural metastability, cation inversion in spinel structure, and order–disorder transition in complex perovskites, which are not shown by the materials synthesized via either conventional ceramic processing or chemistry-based synthesis routes.

(vii) As a result of the fundamentally different phase-forming mechanisms from those of conventional solid state reactions in the conventional ceramic processing, mechanical activation can skip transitional and impurity phases, which are largely concerned with functional and electroceramic materials with complex perovskite, spinel, and layered perovskite structures.

(viii) Mechanical activation can be employed to synthesize several nanocrystalline ceramic materials that cannot possibly be synthesized via either conventional ceramic or chemistry-based processing routes.

(ix) As a result of the nanocrystallinity and ultrafine particle sizes, ceramic materials derived from mechanical activation exhibit a much lowered sintering temperature. For example, $PbZr_{1-x}Ti_xO_3$ (PZT) derived from mechanical activation can be sintered at a temperature as low as 1000 °C [32].

(x) There are a number of unique phenomena that have been observed in association with mechanical activation, including extension of solubility [33], formation of metastable structures [34], amorphization of a crystalline phase [35], phase transition [36, 37] order–disorder transformation [38], cation inversions [26], and crystallization from amorphous states and amorphous precursors [39–41].

5. NANOCRYSTALLINE CERAMICS BY MECHANICAL ACTIVATION

In syntheses of nanocrystalline ceramic materials by mechanical activation, one or more chemical reactions, phase transformations, decompositions, and nucleation and subsequent crystallite growth are associated with mixing, deformation, fracture, refinement, and amorphization of the starting materials, leading to formation of a product phase, with or without the need for further thermal activation at elevated temperatures. In comparison with the solid-state reaction in conventional ceramic processing at high temperatures, a distinct feature of mechanical activation is the realization of particle and crystallite sizes in the nanometer ranges. Nanocrystalline ceramic particles of as fine as 4 nm in size and varying particle morphologies (rounded, rodlike, and platelike) can be synthesized [42]. Several types of chemical reactions can be triggered by mechanical activation, including displacement reaction [43], oxidation [44], reduction [45], decomposition [46], and incipient reaction [47]. Depending on the nature of the starting material and experimental parameters chosen for mechanical activation, phase-formation mechanisms during mechanical activation can be fundamentally different from those in thermal activation.

Several very different phase formation mechanisms have been suggested for ceramic materials triggered by mechanical activation, including various mechanochemical reactions at the interface in microsecond or nanosecond duration of shock, impact, and collision in a highly activated state [37], local temperature-facilitated solid state reactions [39], nucleation at interface [40], and nucleation from the highly activated matrix and subsequent growth of crystallites [48]. It is commonly believed that mechanical activation can significantly increase the reactivity of a solid system, as a result of the refinement in particle and crystallite sizes and creation of various structural and surface defects, and therefore diffusion and reaction kinetics are enhanced. This is supported by the much lowered reaction and phase formation temperatures that are brought about by mechanical activation. Mechanical activation can lead to a significant departure from the equilibrium state. In some cases, the free energy level raised by mechanical activation is above that of an amorphous state. The much refined particle and crystallite sizes, with or without presence of structure defects, enable chemical reactions which otherwise require high temperatures to occur. Thermodynamically, this is accounted for by the energy accumulation process during mechanical activation. A further contribution to the enhanced reactivity is the alleviation, if not elimination, of the diffusion barrier generated by the product phase that separates the reactants.

High temperature and pressure at the collision points can give rise to a new and product phase, although the overall temperature of the mechanical activation chamber normally does not exceed 100 °C in most cases. However, it is questionable whether the short interval of *in-situ* temperature at the collision points, which may be high enough to trigger many types of solid state reaction, will be sufficient for formation of a product phase of several nanometers in dimensions. In discussing the mechanisms of incipient reaction at solid–solid boundary under mechanical stresses, Senna [49] outlined the importance of coordination states, symmetry disturbance, and change in electronic states. Similarly, Boldyrev and Tkacova [2] considered the increase in solid density under a hydrostatic loading, which can cause a decrease in the width of forbidden band and conduction states. The process can be further facilitated by an appropriate combination of hydrostatic stress and shear component, which apparently occur in certain mechanical activation processes. One of the common features in all mechanical activation processes is the involvement of strain, which manifests itself by the shift of atoms from their equilibrium positions and the change in bond lengths and angles. Therefore, structural defects, amorphization and metastable states often occur prior to formation of the product phase with increasing degree of mechanical activation.

There is no doubt that the significant refinement in particle and crystallite sizes during the initial stage of mechanical activation creates newly formed, clean surfaces, which can quickly absorb and react with species that are in direct contact. In the presence of moisture or a liquid phase, hydrothermal processes can occur at the collision points, which can also lead to formation of a product phase [50]. This belief has encouraged the attempt to combine mechanical activation and hydrothermal reaction. In recent studies of mechanical activation for synthesis of electroceramic materials of complex perovskite structure [48], where multiple oxides are involved as the starting materials, a completely different phase formation process has been observed. Nucleation of nanocrystallites of perovskite structure occurs in a highly activated oxide matrix, where a significant refinement in particle and crystallite sizes together with a degree of amorphization have taken place. Subsequent growth of the nanocrystallites with further mechanical activation is a consequence of the equilibrium between the activation-driven buildup and destruction involving the entire masses of nanocrystallites. Constant collisions and rearrangement of nanocrystallites provided by mechanical activation create opportunities for two or more of them to meet at favorable positions leading to growth in the crystallite size. At the same time, there is also a probability that the nanocrystallites are distorted and fragmented by mechanical activation.

While the phase-formation mechanisms and physical phenomena in many systems have yet to be properly understood, numerous nanocrystalline ceramic materials have been successfully synthesized by mechanical activation. They include simple oxides, such as Al_2O_3, ZrO_2, Fe_2O_3, ZnO, and CeO_2, complex oxides of perovskite structure, spinel structure, aurivillius type compound and layered perovskite structure and their solid solutions, nonoxide ceramics such as nitrides, carbides, oxynitrides, sulphides, and ceramic nanocomposites. Table 1 lists examples of the typical nanocrystalline ceramic materials synthesized by mechanical activation. In the following, a brief review is given to each of these major types of nanocrystalline ceramic materials synthesized by mechanical activation.

5.1. Simple Ceramic Oxides

A large number of simple oxides, examples of which include Al_2O_3 [51], ZrO_2 [52–54], Fe_2O_3 [55], Gd_2O_3 [56], CeO_2 [57], SnO_2 [58], ZnO [59], Cr_2O_3 [60], Nb_2O_5 [60], and TiO_2 [61], have been synthesized by mechanical activation. Starting with an inorganic salt, such as chloride, an oxide can be realized by a simple replacement reaction during mechanical activation, followed by a calcination/annealing at temperatures in the range of 150 to 600 °C. To synthesize nanocrystalline Al_2O_3, for example [51], an appropriate powder mixture of $AlCl_3$ and CaO is mechanically activated, followed by calcination at progressively rising temperatures, leading to formation of γ-Al_2O_3 within $CaCl_2$ matrix at 350 °C and then α-Al_2O_3. Nanocrystalline Al_2O_3 particles are then recovered by washing off $CaCl_2$. Similarly, nanocrystalline ZrO_2 [52] particles are produced by mechanical activation of $ZrCl_4$ together with CaO (NaOH and LiOH can also be used) and the subsequent thermal annealing at 300 °C, leading to formation of zirconia particles of 5 to 10 nm in size and of metastable cubic structure. Other examples of simple oxides that have been successfully synthesized by the replacement reaction triggered by mechanical activation include Fe_2O_3, Gd_2O_3, CeO_2, SnO_2, and ZnO, where the starting chemicals are corresponding chlorides in combination with an alkaline or oxide of an alkaline earth. Transitional and metastable phases may well be involved in some cases. For example [55], FeOOH can occur prior to formation of α-Fe_2O_3 during mechanical activation of $FeCl_3$ together with $Ca(OH)_2$ and subsequent thermal annealing with rising temperature. To further modify the particle size and degree of particle aggregation of nanocrystalline oxides derived from mechanical activation, dispersion/dilution agents, such as NaCl and $CaCl_2$, have been proven effective.

In an analog to formation of simple oxides by thermal decomposition of corresponding hydroxides, decomposition of several hydroxides is obtainable by mechanical activation, leading to formation of nanocrystalline particles. For example, mechanical activation of Zr-hydroxides [62] results in formation of nanocrystalline zirconia particles of 4 to 10 nm

Table 1. Examples of typical nanocrystalline ceramic materials synthesized by mechanical activation.

Nanocrystalline ceramics	Size range	Ref.
α-Al_2O_3	~15 nm	[67]
	~100 nm	[68]
α-Al_2O_3, $TiAl_3$, Fe_4Al_{13}	5–15 μm	[72]
α-Al_2O_3/TiN	<10 nm	[148]
γ-Al_2O_3	10–20 nm	[51]
Al_2TiO_5	~50 nm	[97]
$BaFe_{12}O_{19}$	~50 nm	[126, 127]
$BaTiO_3$	10–15 nm (crystallite size)	[74]
	16–20 nm	[75]
$CaBi_4Ti_4O_{15}$	30 nm	[64]
$CaTiO_3$	20 nm	[105]
CdS	4–8 nm	[157]
CeO_2	8–50 nm	[42]
	>10 nm	[57]
	10 nm	[59]
$CoFe_2O_4$	10–40 nm	[127]
CoO, Co_3O_4, NiO	<20 nm	[44]
Cu_2O	15–30 nm	[45]
Feα-Al_2O_3 and Fe-Ti/α-Al_2O_3	10 nm (crystallite size)	[6]
α-Fe_2O_3	10–50 nm	[55]
	~10 nm	[64]
	10–50 nm	[116]
γ-Fe_2O_3	10–12 nm	[118]
Fe_3O_4	10–15 nm	[117]
	10–20 nm (crystallite size)	[128]
Gd_2O_3	20 nm	[56]
$LaFeO_3$	~100 nm	[100]
$MgFe_2O_4$	15 nm	[135]
$MgTiO_3$	11–12 nm	[76]
$MnFe_2O_4$	9.5–40 nm	[132]
	~82 nm	[134]
α-$MoSi_2$	88 nm	[10]
$NiFe_2O_4$	8.05 nm	[26]
	6 nm (crystallite size)	[121]
	10 nm	[127]
	15 nm	[135]
$Pb(Sc_{1/2}Ta_{1/2})O_3$	7–10 nm (crystallite size)	[161]
$Pb(Zr_{0.52}Ti_{0.48})O_3$	20–40 nm	[32]
	30–50 nm	[159]
$PbNb_2O_6$	10–15 nm (crystallite size)	[160]
$PbTiO_3$	16.5 nm	[78]
PMN	~15 nm (crystallite size)	[81]
0.4PMN-0.6PMW	7–12 nm	[38]
PMN-PZN-PT	5–10 nm (crystallite size)	[89]
PZN	10–15 nm (crystallite size)	[90]
SiC	20–30 nm	[13]
SnO_2	20–30 nm (crystallite size)	[58]
	40 nm	[59]
$SrBi_4Ti_4O_{15}$	~50 nm	[63]
TiN	9 nm	[7]
TiN/TiB_2	5–10 nm	[145]
WC/MgO	4–20 nm	[147]
$ZnFe_2O_4$	20 nm	[21]
	15–20 nm	[22]
	11 nm	[119]
	8–10 nm	[120]
	40 nm	[133]
ZnO	20 nm	[63]
	28 nm	[59]
ZnS	~16 nm	[156]
ZrN	14 nm	[7]
ZrO_2	6 nm	[42]
	5–10 nm	[52]
	9–13 nm	[53]
	49 nm (dry activation)	[54]
	14 nm (wet activation)	
	15–42 nm	[62]
	0.1–1.5 μm	[65]
ZrSi	45 nm (crystallite size)	[158]
$ZrSi_2$	23 nm (crystallite size)	[158]

in sizes and of metastable tetragonal structure, in contrast to the monoclinic structure for ZrO_2 particles derived from thermal annealing of the hydroxide precursor. This is apparently related to the much refined crystallite size derived from mechanical activation, where the crystallite coarsening and particle aggregation that are always observed at a calcination temperature as low as 500 °C are avoided. Other successful examples of mechanical activation in decomposing ceramic precursors include ZnO [63] and Fe_2O_3 [64]. For example, zinc oxide particles of 10 to 20 nm in size were successfully obtained, when zinc nitrate hydroxide hydrate precursor, ($Zn_5(NO_3)_2(OH)_8{\cdot}2H_2O$), was mechanically activated in NaCl for 15 hours, where NaCl was used as a drying and dispersion agent [63]. Several decomposition steps were triggered by mechanical activation prior to nucleation and subsequent growth of ZnO particles with increasing degree of mechanical activation. The nanocrystalline ZnO particles thus synthesized exhibited a well-established hexagonal morphology and are almost agglomeration-free, which were compared favorably with those derived from conventional calcination of the same precursor at 400 °C.

Extraction of zirconia from zircon, which is the principal mineral source for zirconia, is traditionally carried out at very high temperatures. When mechanically activated with calcium and magnesium [65], zircon undergoes decomposition to form zirconia and Ca- or Mg-silicates. Similarly, zirconia can be produced by mechanical activation of zircon together with oxides of alkaline earth metals [65]. Unlike the zirconia phase derived from high temperature calcination, nanocrystalline zirconia particles thus produced exhibit a metastable tetragonal structure, which undergoes phase transformation into monoclinic upon heating up to 1200 °C. The occurrence of metastable tetragonal structure is apparently related to the fine nanocrystallites derived from mechanical activation.

Alumina (Al_2O_3), which is one of the most studied ceramic materials and is widely employed in numerous structural and functional applications, is traditionally derived from bauxite, for example by the Bayer process [66] involving digestion and calcination at high temperatures. There exist several transitional phases of aluminum hydroxides/hydrates and oxides, which normally occur prior to formation of thermodynamically stable α-Al_2O_3 at a high enough calcination temperature. On the one hand, as a result of the enhanced reactivity of bauxite brought about by mechanical activation, the extraction rate of aluminum hydroxides from bauxite is significantly improved in the Bayer process. On the other hand, in the search for alternative routes for the aluminum hydroxide/hydrate to alumina conversion, which is traditionally realized by calcination at high temperatures, mechanical activation has been attempted by several investigators. To date, the experimental observations reported by different research groups are rather sketchy. For example, an identical sequence of phase transitions to those commonly observed in calcination of gibbsite was reported by Tonejc et al. [67], who employed high energy ball milling for mechanical activation, while others observed a rather different sequence of phase transitions between mechanical activation and thermal activation. These differences are accountable for by the differences in experimental setup and experimental parameters employed by different investigators. In a recent study conducted by Yong and Wang on gibbsite [68], it was observed that mechanical activation of monoclinic gibbsite [$Al(OH)_3$] in nitrogen led to formation of nanocrystalline boehmite (AlOOH) of orthorhombic structure, which cannot be converted into alumina by prolonging the mechanical activation process. Nanocrystalline boehmite phase started to appear at merely 3 hours of mechanical activation followed by a steady development in both phase purity and crystallite size with increasing mechanical activation time. Forty hours of mechanical activation produced in an essentially single-phase boehmite, together with nanocrystallites of α-Al_2O_3 of 2 to 3 nm in sizes dispersed in the boehmite matrix. Upon subsequent thermal annealing, mechanically activated boehmite transformed to γ-Al_2O_3 at 520 °C and then to α-Al_2O_3 at around 1100 °C. The fine α-Al_2O_3 particles thus produced are 100 to 200 nm in size and exhibit a rounded particle morphology. This is in contrast to the calcination temperature of 1400 °C required for gibbsite that was not subjected to any mechanical activation, which undergoes transition at above 220 °C to boehmite and then to transitional phases of δ-Al_2O_3 and θ-Al_2O_3, prior to formation of α-Al_2O_3.

There are a number of other types of reaction that can be triggered by mechanical activation and lead to formation of simple oxides of nanocrystallinity. For example, CoO and NiO nanoparticles [44] can be formed by mechanical activation of corresponding metal elements in a highly oxidizing environment, where the oxidation is speeded up by mechanical activation. mechanical activation of Fe_3O_4 together with Al [69] leads to formation of a mixture of α-Al_2O_3, $FeAl_2O_4$, and α-Fe. Reduction reaction of $FeTiO_3$ by Si is obtainable at room temperature by mechanical activation [70, 71], leading to formation of nanocrystalline TiO_2 in an amorphous SiO_x, together with intermetallic compounds and α-Fe, depending on Si content in the starting mixture. These mechanical activation-driven processes consist of an initiation stage and subsequent reaction stage, where the length of initiation stage and subsequent reaction rate are largely controlled by the mechanical activation intensity. A similar mechanochemical reaction [72] has been reported for between $FeTiO_3$ and Al during mechanical activation, producing nanocrystalline Al_2O_3 together with intermetallic phases of $TiAl_3$ and Fe_4Al_{13}.

5.2. Complex Ceramic Oxides

A number of complex oxides of nanocrystallinity, including those of perovskite structure, complex perovskite structure, aurivillius type and layered perovskite structure, and spinel structure and their solid solutions, have been successfully synthesized by mechanical activation of either constituent oxides or ceramic precursors, such as hydroxides and oxalates, or a mixture of these. Depending on the nature of the starting materials and the experimental setup for mechanical activation, there can be considerable differences in the types of mechanochemical reaction involved and the phase-formation steps during mechanical activation. In several cases, complex oxides of nanocrystallinity are formed as a result of one single step of mechanical activation, while in others a subsequent thermal annealing step is required before designed nanocrystalline ceramic phases are realized. As a consequence of the enhanced reactivity brought about by mechanical activation, phase-formation temperature for complex oxides can be significantly lowered.

Among the complex oxides of nanocrystallinity that have been successfully synthesized by mechanical activation, alkaline earth titanates, such as $BaTiO_3$ and $SrTiO_3$, exhibit a perovskite structure. $BaTiO_3$, which is one of the most widely used electroceramic materials for numerous applications in electronics and microelectronics, is traditionally synthesized by the solid-state reaction between TiO_2 and $BaCO_3$ at temperatures above 1000 °C [73]. The conventional solid-state reaction between TiO_2 and $BaCO_3$ at high temperatures is associated with several fatal disadvantages. For example, the interfacial reaction between TiO_2 and $BaCO_3$ is accompanied by several intermediate phases, which often occur as unwanted impurity phases together with the product phase of $BaTiO_3$. The high calcination temperature that is required by phase formation in the solid state reaction always results in unwanted particle coarsening and aggregation, the presence of which adversely affects subsequent sintering and densification of $BaTiO_3$. It is therefore both scientifically interesting and technologically demanding to search for alternative synthesis routes for $BaTiO_3$. In an attempt to synthesize nanocrystalline $BaTiO_3$ of perovskite structure, Xue et al. [74] carried out mechanical activation of TiO_2 and BaO in a nitrogen atmosphere, leading to steady formation of $BaTiO_3$ of 10 to 15 nm in crystallite sizes. Employment of the nitrogen atmosphere is to stop BaO from reaction with CO_2 in air. In addition to BaO as the source material for Ba in $BaTiO_3$, $Ba(OH)_2{\cdot}8H_2O$ was also used [75]. When mechanically activated together with TiO_2 in acetone, nanocrystallites of $BaTiO_3$ steadily resulted. The crystallinity of thus derived $BaTiO_3$ was further enhanced by subsequent thermal annealing. There are several other examples of nanocrystalline titanates that have been synthesized by mechanical activation, including $MgTiO_3$ [76, 77] and $PbTiO_3$ [78–80]. For example, mechanical activation of PbO and TiO_2 at room temperature led to formation of $PbTiO_3$ (PT) of perovskite structure and nanocrystallinity. Figure 1 is a transmission electron microscopy (TEM) micrograph showing the nanoparticles of PT derived from mechanical activation of the constituent oxides at room temperature. They are 5 to 10 nm in size and spherical in particle morphology. While $PbTiO_3$ was nucleated in the

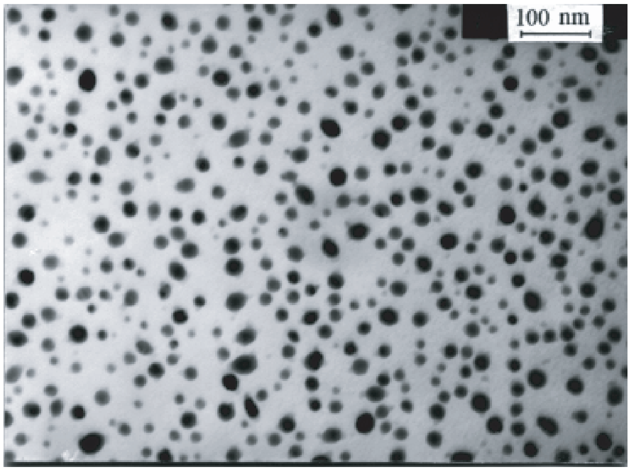

Figure 1. A bright field TEM micrograph showing the nanoparticles of lead titanate ($PbTiO_3$) synthesized by mechanical activation of PbO and TiO_2 at room temperature.

highly activated matrix of oxides, strong deviation from compositional stoichiometry, vacancy generation, and occupation of B-sites by Pb^{2+} in the perovskite structure may well occur during mechanical activation.

Lead zirconate titanate (PZT), which is the classical piezoelectric, has recently been synthesized by mechanical activation of constituent oxides of PbO, ZrO_2, and TiO_2 at room temperature [32]. Unlike in the solid state reaction of these oxides at high temperatures, transitional $PbZrO_3$ (PZ) and PT phases were not observed during mechanical activation of these oxides. This represents a significant step forward in synthesizing this technologically demanding material for a number of applications in sensors, transducers, and actuator devices using the low-cost oxides as starting materials. As will be discussed later, the phase-formation process of complex perovskites during mechanical activation is fundamentally different from that in the conventional solid-state reaction, where the process is controlled by one or more interfacial diffusions and reactions. In contrast, mechanical activation triggered the nucleation and subsequent crystallite growth of complex perovskites in a highly activated matrix of oxide composition. Owing to the unique nanocrystalline structures of PZT derived from mechanical activation, they can be sintered to a >99% theoretical density at a temperatures as low as 1000 °C, which is about 200 °C lower than what is normally required for this classical piezoelectric.

Another most remarkable example of mechanical activation in synthesizing nanocrystalline electroceramic materials of complex perovskite structure is PbO-based relaxor ferroelectrics [81]. $Pb(Mg_{1/3}Nb_{2/3})O_3$ (PMN), for example, is a relaxor-type ferroelectric of perovskite structure exhibiting some of the most desirable dielectric and electrostrictive properties for a number of applications in sensors and actuators [82]. Behind PMN, there is a big family of Pb-based relaxor ferroelectrics, typical examples of which are $Pb(Mg_{1/3}Nb_{2/3})O_3$–$Pb(Zn_{1/3}Nb_{2/3})O_3$ (PMN–PZN) and $Pb(Mg_{1/3}Nb_{2/3})O_3$–$Pb(Zn_{1/3}Nb_{2/3})O_3$–$PbTiO_3$ (PMN–PZN–PT). Constituent oxides are undoubtedly the starting materials of lowest cost for these relaxor ferroelectrics. It is, however, impossible to synthesize a single phase PMN and PMN-based relaxor ferroelectrics of perovskite structure from their constituent oxides by one-step solid-state reaction at high temperatures [83]. Calcination of a powder mixture of PbO, MgO, and Nb_2O_5, for example, always produces one or more transitional pyrochlore phases (notably $Pb_3Nb_4O_{13}$ and $Pb_2Nb_2O_7$), prior to formation of perovskite PMN phase. On the one hand, this is related to the difference in reactivity among the three oxides over a wide range of temperatures. On the other hand, there apparently exists a much larger interfacial area between any two of these three oxides than the common contact area where all three oxides are present, creating opportunities for the preferred interfacial reaction between PbO and Nb_2O_5 to take place [84]. To overcome the much unwanted pyrochlore phases in PMN and PMN-based relaxors, multiple steps of calcination and postcalcination communition are necessary in the well known Columbite method [83].

Figure 2 shows the X-ray diffraction (XRD) traces of mixed oxides of PbO, MgO, and Nb_2O_5 upon mechanical

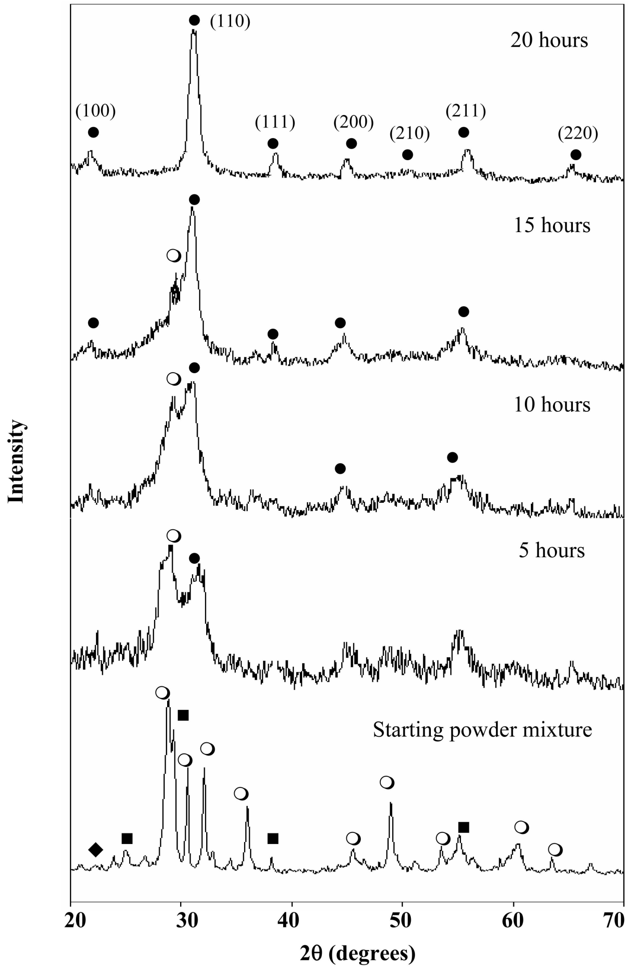

Figure 2. XRD patterns of mixed oxides of PbO, MgO, and Nb_2O_5 mechanically activated for various time periods from 0 to 20 hours. O: PbO, ■: Nb_2O_5, ♦: MgO, •: PMN. Reprinted with permission from [85], J. Wang et al., *Solid State Ionics* 124, 271 (1999). © 1999, Elsevier Science.

activation for various time periods up to 20 hours [85]. Sharp peaks of crystalline PbO, MgO, and Nb_2O_5 are observed for the starting oxide mixture, indicating that little or no reaction took place during the conventional ball milling, which was employed for mixing of the constituent oxides. A few broadened peaks were observed when the oxide mixture was mechanically activated for 5 hours. The strongest one at a 2θ angle of $\sim$29.1° corresponds to the PbO (111) peak, which was seen as a sharp one before mechanical activation. This implies that the initial 5 hours of mechanical activation led to a significant refinement in particle and crystallite sizes, together with a degree of amorphization of constituent oxides. This is supported by a rise in the specific surface area from 1.20 m^2/g for the oxide mixture that was not subjected to mechanical activation to 9.52 m^2/g for the powder composition subjected to 5 hours of mechanical activation. The second strongest broadened peak at a 2θ angle of $\sim$31.2° and those at 2θ angles of 44.7 and 55.5° are newly formed. They are assigned to perovskite PMN (110), (200), and (211) peaks, respectively, suggesting that nanocrystallites of perovskite PMN phase had been formed as a result of the initial 5 hours of mechanical activation. The intensity of the perovskite PMN (110) peak increases with increasing mechanochemical treatment time, at the expense of the PbO (111) peak. In the composition mechanically activated for 20 hours, nanocrystalline PMN is the only XRD-detectable phase, as confirmed by the well defined peaks at 2θ angles of 21.9, 31.2, 38.5, 44.7, 50.2, 55.5, and 65.0°, respectively. There is also an apparent sharpening in PMN (110), (111), (200), (210), and (211) peaks when the mechanical activation time is extended to 20 hours, demonstrating that there is an increase in the crystallinity of perovskite PMN phase. Calculation using the Scherrer equation [86] on the basis of peak broadening of the perovskite (110) peak showed that the PMN nanocrystallites exhibited an average crystallite size of $\sim$15 nm upon 20 hours of mechanical activation, in comparison to $\sim$9 nm for the powder composition that was mechanically activated for 5 hours. Figure 3 is a bright field TEM micrograph showing the PMN nanoparticles that were synthesized by mechanical activation at room temperature of constituent oxides. Pyrochlore phases, such as $Pb_3Nb_4O_{13}$ and $Pb_2Nb_2O_7$ that are always observed as transitional phases in the temperature-driven solid-state reaction, are apparently not involved prior to formation of perovskite phase, while the perovskite nanocrystallites of lead magnesium niobate underwent a steady growth with increasing degree of mechanical activation.

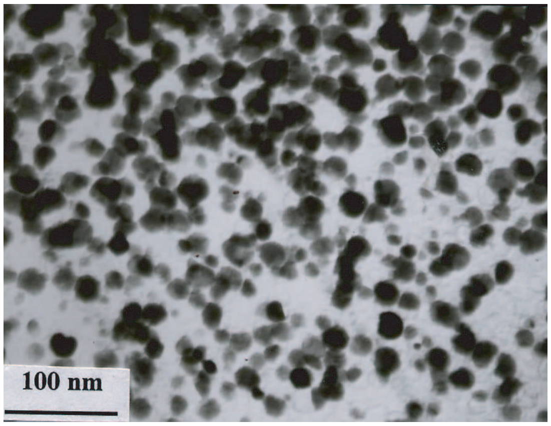

Figure 3. A bright field TEM micrograph showing the nanoparticles of lead magnesium niobate that were synthesized by mechanical activation of constituent oxides at room temperature.

It has been established that phase formation of PbO-based relaxor ferroelectrics from constituent oxides triggered by mechanical activation is not a result of one or more interfacial reactions as stated by the Roller model [87]. Instead, they occur via a nucleation process involving all three oxides in a highly activated oxide matrix, where a significant refinement in particle and crystallite sizes together with a degree of amorphization had taken place. There is a much smaller amount of common contact areas involving all oxides than the interfacial contact areas between any two of them (e.g., between PbO and Nb_2O_5 particles). On the one hand, this, together with the high reactivity between PbO and Nb_2O_5, accounts for the occurrence of transitional pyrochlore phases in the conventional solid-state reaction when mixed oxides of PbO, MgO, and Nb_2O_5 are calcined at elevated temperatures. On the other hand, it is very unlikely that the formation of nanocrystallites of perovskite PMN phase triggered by mechanical activation is a result of the interfacial reactions involving all three oxides without first going through any of the transitional pyrochlore phases. The subsequent steady growth of PMN nanocrystallites of perovskite structure with increasing mechanical activation time is a consequence of the equilibrium between activation-driven buildup and destruction involving the entire masses of perovskite nuclei [88]. Constant collisions and rearrangement of perovskite nuclei provided by mechanical activation create opportunities for two or more of these nuclei to meet at favorable positions leading to growth in crystallite size. At the same time, there is also a probability that the perovskite nanocrystallites are distorted and fragmented by mechanical activation.

Nucleation and subsequent growth of perovskite nanocrystallites triggered by mechanical activation of constituent oxides have also been observed in a number of PMN-based relaxor ferroelectrics. For example, mechanical activation of mixed oxides of PbO, MgO, ZnO, TiO_2, and Nb_2O_5 equivalent to stoichiometric composition of $0.9\cdot[0.4Pb(Mg_{1/3}Nb_{2/3})O_3–0.6Pb(Zn_{1/3}Nb_{2/3})O_3]–0.1PbTiO_3$ led to formation of perovskite nanocrystallites [89]. The multiple oxide composition would maximize the involvement of several transitional phases prior to formation of perovskite PMN–PZN–PT nanocrystallites, if phase formation triggered by mechanical activation proceeded via one or more interfacial reactions. In other words, it would be almost impossible not to go through one or more transitional phases if the phase formation of activation-triggered perovskite nanocrystallites is controlled by one or more interfacial reactions, while the chance to involve all five oxides at an interfacial location is minimum. Phase analyses at various stages of mechanical activation, however, demonstrated that no intermediate phases occurred prior to nanocrystalline PMN–PZN–PT phase with increasing mechanical activation time. A single perovskite phase was obtained at 20 hours of mechanical activation. Figure 4 is a high resolution TEM (HRTEM) micrograph together with the selected

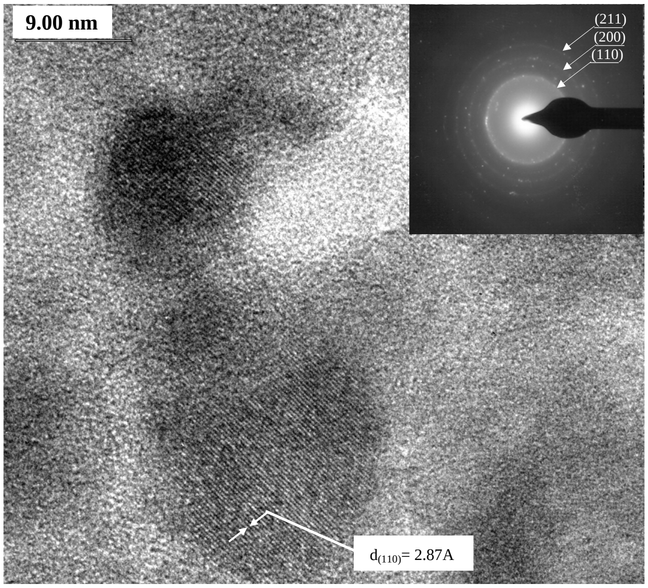

Figure 4. A HRTEM micrograph together with the selected area diffraction patterns showing the nanocrystallites of perovskite PMN–PZN–PT in an amorphous matrix triggered by 10 hours of mechanical activation. Reprinted with permission from [48], J. Wang et al., *J. Solid State Chem.* 154, 321 (2000). © 2000, Elsevier Science.

area diffraction patterns showing the nanocrystallites of perovskite PMN–PZN–PT in an amorphous matrix triggered by 10 hours of mechanical activation [48]. They are well established perovskite crystallites of 5 to 10 nm in dimension dispersed in an amorphous oxide matrix. Measurement of lattice spacing (e.g., $d_{110} = 2.87$ Å) confirmed that these nanocrystallites were perovskite PMN–PZN–PT.

Mechanical activation is successful in synthesizing complex perovskites of nanocrystallinity that cannot possibly be synthesized by any other processing techniques. For example, $Pb(Zn_{1/3}Nb_{2/3})O_3$ is a relaxor ferroelectric exhibiting a partially disordered perovskite structure and showing many of the most desirable dielectric and piezoelectric properties for a number of applications in sensors and actuators. However, the pursuit to synthesize a $Pb(Zn_{1/3}Nb_{2/3})O_3$ (PZN) of perovskite structure via both traditional ceramic and chemistry-based novel processing routes over the last three decades has failed. The difficult-to-synthesize nanocrystallites of PZN have, however, been successfully synthesized by mechanical activation of either constituent oxides of PbO, ZnO, and Nb_2O_5 or a mixture of PbO and prereacted $ZnNb_2O_6$ from ZnO and Nb_2O_5 [90]. The activation-derived PZN exhibits a well established perovskite structure and a crystallite size in the range of 10 to 15 nm.

Bismuth titanate ($Bi_4Ti_3O_{12}$ or BIT) and bismuth titanate-based electroceramics are examples of layered perovskites that have been successfully synthesized by mechanical activation. These electroceramic materials, which exhibit a high Curie temperature (~675 °C for BIT) and excellent piezoelectric and dielectric properties, are promising candidates for high temperature piezoelectric and ferroelectric applications [91]. They are traditionally prepared by solid-state reaction among the constituent oxides at elevated temperatures. However, due to the high volatility of Bi_2O_3 at elevated temperatures, it is rather difficult to synthesize a bismuth-based ceramic of stoichiometry by the conventional solid-state reaction. Several bismuth titanate-based functional ceramics, including $Bi_4Ti_3O_{12}$ [92], $SrBi_4Ti_4O_{15}$ [93], and $CaBi_4Ti_4O_{15}$ [94], have been synthesized by mechanical activation of mixed oxides at room temperature. Figure 5 shows the XRD traces of starting oxide mixture of SrO, Bi_2O_3, and TiO_2 together with those mechanically activated for 5, 10, 15, and 20 hours, respectively [93]. Sharp peaks of crystalline Bi_2O_3 and TiO_2 are observed with the starting oxide mixture, while SrO is not detected by XRD due to the relatively small amount involved. Upon 5 hours of mechanical activation, XRD peaks of these oxides are broadened. The small peak at a 2θ angle of 30.5° is newly formed, which is assigned to the $SrBi_4Ti_4O_{15}$ (SBIT) (119) plane, indicating the formation of nanocrystalline SBIT by mechanical activation for 5 hours. Almost all the sharp peaks of oxides have vanished in the composition mechanically activated for 10 hours, and they are replaced by a few broadened ones. The Bi_2O_3 (120) peak, which is seen as a sharp one in the powder mechanically activated for 5 hours, has broadened considerably. The disappearance of sharp peaks for oxides and subsequent formation of broadened peaks, with increasing mechanical activation time, suggest that a significant

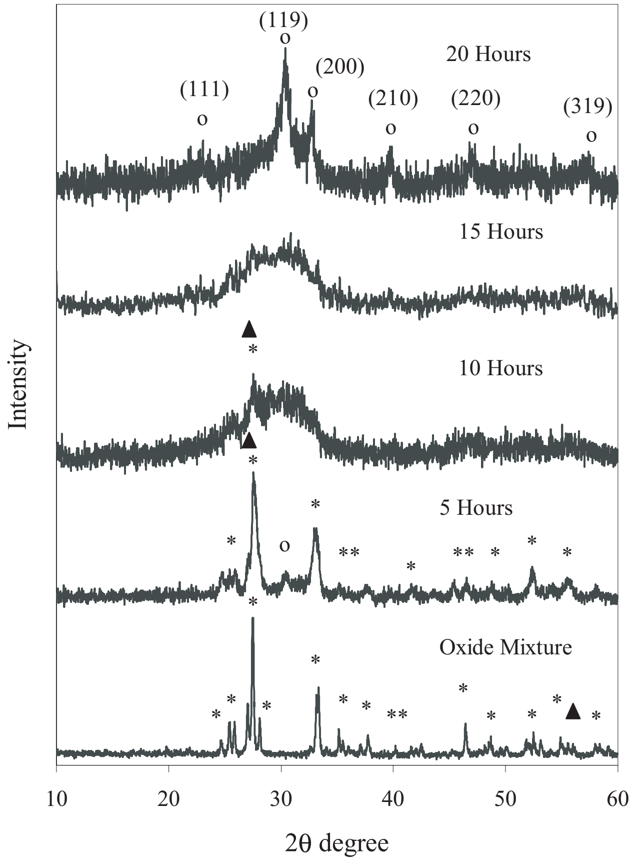

Figure 5. XRD patterns of the mixed oxides of Bi_2O_3, TiO_2, and SrO equivalent to SBIT subjected to mechanical activation for various time periods ranging from 0 to 20 hours. ∗: Bi_2O_3, ▲: TiO_2, ∘: SBIT. Reprinted with permission from [93], S. H. Ng et al., *Mater. Chem. Phys.* 75, 131 (2002). © 2002, Elsevier Science.

refinement in particle and crystallite sizes, together with a degree of amorphization of mixed oxides, took place at the initial stage of mechanical activation. This is followed by nucleation and subsequent growth of SBIT nanocrystallites. As shown in Figure 5, diffraction peaks at 2θ angles of 23.1, 30.5, 39.8, 47.2, and 57.2° are established for the composition mechanically activated for 20 hours. They correspond to SBIT (111), (119), (0210), (220), and (319) planes, respectively, of the layered perovskite phase.

There are a number of other complex oxides of nanocrystallinity that have been successfully synthesized by mechanical activation of either constituent oxides or chemical precursors or a mixture of the two. They include $La_{0.7}Sr_{0.4}\cdot MnO_3$ from constituent oxides of La_2O_3, SrO, and MnO_2 [95], $LaMnO_3$ from La_2O_3 and Mn_2O_3 [96], Al_2TiO_5 from Al_2O_3 and TiO_2 [97], $Sn_{0.5}Ti_{0.5}O_2$ from TiO_2 and SnO [98], Bi_3NbTiO_9 from Bi_2O_3, Nb_2O_5, and TiO_2 [99], $LaFeO_3$ from La_2O_3 and Fe_2O_3 [100], $LiCoO_2$ from $LiOH\cdot H_2O$ and $Co(OH)_2$ [101], $ZrTiO_4$ from ZrO_2 and TiO_2 gels [102], $LiMn_2O_4$ from MnO_2 with LiOH [103], $MgAl_2O_4$ from $Mg(OH)_2$ and $Al(OH)_3$ [104], $CaTiO_3$ from CaO and TiO_2 [105], $Sr_3Ti_2O_7$ from SrO or $SrCO_3$ or $Sr(OH)_2\cdot 8H_2O$ and TiO_2 [106], $LaCrO_3$ from amorphous $Cr_2O_3\cdot nH_2O$ and La_2O_3 [107], aurivillius type compounds from constituent oxides and precursors [108, 109], and fluorite type phases in the system Bi_2O_3–Nb_2O_5–Ta_2O_5 [110]. Mechanochemical reactions responsible for formation of these oxides are dependent on the nature of starting materials and processing parameters chosen for mechanical activation. For example, mechanical activation of TiO_2 together with $Mg(OH)_2$ triggered an incipient reaction between them in association with dehydration of the hydroxide [111]. Use of hydroxide precursors or hydrated oxides as the starting materials can generate local hydrothermal environments responsible for formation of a product phase.

Silicates constitute a big family in the complex oxides, which are traditionally synthesized by conventional solid-state reaction at high temperatures. Mechanical activation has been applied to synthesis of several technologically demanding silicates, which otherwise require a very high calcination temperature. For example, mullite is a compound formed between alumina and silica at temperatures well above 1000 °C. Mechanical activation of constituent oxides and hydroxides (for example, gibbsite and silica gel) significantly lowers the crystallization of mullite [112], which often occurs via one or more transitional spinel phases in the conventional solid-state reaction. Mechanical activation of MgO and SiO_2 produces a magnesium silicate of low crystallinity similar to what is formed under certain hydrothermal reaction conditions [113]. Magnesium silicate of well established crystallinity is obtained by subsequent thermal annealing. Hydrated calcium silicates can also be synthesized mechanochemically at room temperature where the presence of water and moisture employed play a significant role [114]. Mechanochemical reactions between kaolinite and several oxides (such as ZnO and CaO) and nonoxides have been studied by several investigators. For example, cesium aluminum silicate and intercalation complexes occur as a result of mechanical activation of kaolinite together with CsF [115].

5.3. Nanocrystalline Oxide Ferrites

Nanocrystalline ferrites, magnetite (Fe_3O_4), and maghemite (Y-Fe_2O_3) were among the ceramic materials synthesized by mechanical activation in the early development stage of this novel technique. They were synthesized from corresponding oxides, hydroxides, precursors, and chemicals (such as chlorides) or a mixture of these. The types of mechanochemical reaction leading to formation of nanocrystalline ferrite phases include replacement reaction [116], decomposition [66], oxidation/reduction [117], and mechanical activation-induced nucleation and crystallite growth [118]. Very different magnetic behaviors are observed with these nanocrystalline ferrites derived from mechanical activation, as compared to those of their coarse/bulk counterparts and those materials derived from either conventional ceramic processing or wet-chemistry routes. For example, $ZnFe_2O_4$ and $NiFe_2O_4$ derived from mechanical activation demonstrate a much enhanced magnetization, as a result of the partially inverted spinel structure [26, 119].

Mechanical activation triggers a steady occurrence of nanocrystalline $ZnFe_2O_4$ [120], $NiFe_2O_4$ [121], $MnFe_2O_4$ [122], and Ni–Zn ferrite [123] of particle size in the range of 5 to 20 nm from corresponding oxide mixtures, for example, α-Fe_2O_3 and ZnO for $ZnFe_2O_4$. Subsequent annealing at a temperature in the range of 600 to 800 °C enhances their crystallinity and magnetic properties in association with superparamagnetic to ferromagnetic transition. They can also be synthesized by mechanical activation of corresponding hydroxides, with or without involvement of certain transitional phases such as Fe_3O_4 and γ-Fe_2O_3, depending on the selection of mechanical activation conditions [124]. A replacement reaction is apparently involved in mechanical activation of chlorides, such as $ZnCl_2$ and $FeCl_3$, with NaOH for synthesis of $ZnFe_2O_4$, the crystallinity and magnetic behavior of which are largely controlled by the post-activation thermal annealing [22].

Several different combinations of starting materials have been experimented for synthesis of nanocrystalline $BaFe_{12}O_{19}$ by mechanical activation, including Fe_2O_3 and $Ba(OH)_2$ [125], BaCl and FeCl [126], and co-precipitation-derived hydroxide precursors [127]. Formation of $BaFe_{12}O_{19}$ of high crystallinity and hexagonal platelike morphology requires a postactivation annealing at a temperature in the range of 600 to 800 °C. Transitional phases, such as α-Fe_2O_3, γ-Fe_2O_3, and Fe_3O_4, can occur, prior to $BaFe_{12}O_{19}$, during mechanical activation and subsequent thermal annealing, depending on the nature of starting materials and processing conditions of mechanical activation. For example, when a co-precipitated hydroxide precursor is mechanically activated together with sodium chloride as a dispersion agent, nanocrystallites of α-Fe_2O_3 and spinel γ-Fe_2O_3 of <10 nm in size occurred together with $BaFe_{12}O_{19}$. A single phase $BaFe_{12}O_{19}$ of 50–100 nm in size and of platelike morphology is developed upon subsequent calcination at 800 °C [127]. Using BaCl and FeCl as the starting materials, mechanical activation in NaOH led to formation of a mixture of Fe oxides and hydroxides together with NaCl as a by-product [126]. Nanocrystalline $BaFe_{12}O_{19}$ resulted upon subsequent calcination at 800 °C. Crystallite size and degree of agglomeration of thus derived $BaFe_{12}O_{19}$ can be further tailored by employing NaCl as an effective dispersion agent.

Phase transformations among α-Fe_2O_3, γ-Fe_2O_3, and Fe_3O_4 can be triggered by mechanical activation and are critically dependent on the oxygen partial pressure [128–131]. For example, mechanical activation of α-Fe_2O_3 in vacuum can lead to complete transformation to Fe_3O_4, involving a significant refinement in crystallite size at the initial stage of mechanical activation prior to nucleation and growth of Fe_3O_4 [128]. Mechanical activation of γ-Fe_2O_3 and Fe_3O_4 in air gives rise to formation of α-Fe_2O_3 [132].

Nanocrystalline ferrites derived from mechanical activation demonstrate very different structural and magnetic behaviors. For example, $MnFe_2O_4$ derived from mechanical activation of FeCl together with MnO exhibits a unique core–shell structure, which consists of a ferrimagnotic core surrounded by a spin–glass shell, and therefore there occur a coupling and exchange between the spin in the core and that in the shell [132]. The most remarkable structural feature brought about by mechanical activation in nanocrystalline ferrites is the cation inversion. In bulk ceramic forms, spinel ferrites consist of close-packed face-centered cubic arrays of O anions, with the tetrahedral (A) and octahedral (B) sites partially occupied by metal cations. Due to the specific electronic configurations of cations and types of superexchange interactions among them, their magnetic properties are strongly dependent on the occupancy and exchange of cations in the two sites and among them. Unusual cation distribution has been observed in $ZnFe_2O_4$, $MnFe_2O_4$, and $NiFe_2O_4$ nanoparticles derived from mechanical activation [133–135]. This gives rise to a significant enhancement in magnetization and several other anomalous behaviors, although the exact reasons behind the inversion are yet properly established. Figure 6 [26] is a magnetization hysteresis loop measured at 5 K for $NiFe_2O_4$ particles formed in silica matrix by mechanical activation of a gel precursor, where nanocrystallites of Fe_3O_4 were first nucleated followed by incorporation of Ni^{2+} into Fe_3O_4 leading to formation of $NiFe_2O_4$ nanoparticles of ~8 nm in size. Although magnetization is not saturated at a magnetic field of 9 T due to the surface strain arising from silica matrix, these $NiFe_2O_4$ nanoparticles demonstrate an unusually high magnetization of 74.3 emu/g at 9 T.

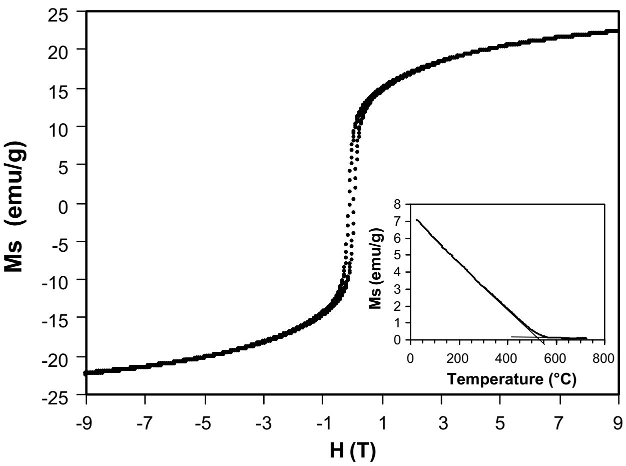

Figure 6. Magnetization hysteresis loop, measured at 5 K, for gel composition of $NiFe_2O_4$ mechanically activated for 30 hours. Inset shows the magnetization as a function of measuring temperature.

In the inverse spinel structure of $NiFe_2O_4$, equal numbers of Fe^{3+} cations in tetrahedral (A) and octahedral (B) sites are coupled in an antiparallel arrangement. The net magnetic moment is therefore originated from the octahedrally coordinated Ni^{2+} cations. Displacement of an A-site Fe^{3+} ion with moment of 5 μ_B by a Ni^{2+} ion with moment of 2.3 μ_B gives rise to an increase in the net moment. The enhancement of magnetization shown in Figure 6 for $NiFe_2O_4$ nanoparticles derived from mechanical activation arises from occupation of Ni^{2+} cations in the tetrahedral sites, which have been confirmed by Raman, Fourier transform infrared, and Mössbauer studies [26, 135]. The cation inversion also explains the shift in Curie temperature from 585 °C for bulk $NiFe_2O_4$ to 530 °C for the nanocrystalline $NiFe_2O_4$ particles. Since the Fe^{3+}(A)–O–Fe^{3+}(B) interaction is the strongest one among those in nickel ferrite [136], any displacement of A site Fe^{3+} will reduce the overall superexchange interaction and hence decrease the Curie temperature. Furthermore, upon displacement of A site Fe^{3+} ions by Ni^{2+} ions, O^{2-} anions in the A sites are forced to shift in the direction to give space to Ni^{2+} ions of larger ionic radii. This leads to reduction in the cation(A)–O–cation(B) bond angles and hence weakens the superexchange interaction.

The observed disorder of cations for nanocrystalline $NiFe_2O_4$ particles formed *in-situ* in silica matrix by mechanical activation occurs in conjunction with the phase formation process. As discussed, initial mechanical activation led to nucleation of Fe_3O_4 nanocrystallites, which was followed by the incorporation of Ni^{2+}. Site occupancy of cations are affected by a combination of a number of parameters. Although Ni^{2+} possesses a high octahedral site preference energy, the electrostatic energy favors a normal spinel arrangement, as $NiFe_2O_4$ has a deformation parameter μ of 0.3823. The normal spinel configuration is more stable when $\mu > 0.379$ [136]. Very often, however, the difference in total energy between the normal and inverse spinel distributions is very small. Therefore, when Ni^{2+} approaches an octahedral site that has already been occupied by Fe^{2+}, which also possesses a high octahedral site preference energy, it will be forced to occupy one of the nearest tetrahedral sites. This is particularly so when the incorporation of Ni^{2+} was triggered by mechanical activation, which can only promote short-range diffusion [137]. Ni^{2+} then displaces the Fe^{3+} cations if the nearest tetrahedral sites are preoccupied by Fe^{3+} cations, which have zero octahedral site preference energy.

5.4. Carbides, Nitrides, Nonoxides, and Nanocomposites

In parallel to the success of synthesizing ceramic oxides and complex oxide ceramics of nanocrystallinity, mechanical activation has been successfully applied to synthesis of several nonoxide ceramics, including carbides, nitrides, borides, and ceramic nanocomposites [12, 13, 138–144]. In several cases, mechanical activation of metallic elements together with carbon (graphite) and boron in a nitrogen environment produce corresponding carbides, borides, and nitrides. For example, TiC [141] and TiB_2 [142] can be synthesized by mechanical activation of powder mixtures of elemental Ti and C and Ti and B, respectively, in a planetary ball mill using tungsten carbide balls as the activation media. The phase formation steps during mechanical activation consisted of diffusion of carbon or boron into titanium in the initial stage, whereby a small amount of TiC and TiB_2 was formed, followed by the mechanically triggered self-propagating reaction. Titanium nitride is produced by mechanical activation of titanium in nitrogen gas, where the reaction proceeded via a surface reaction between titanium particles and nitrogen and then diffusion of nitrogen into titanium under mechanical activation [143]. Nitridation of silicon at high temperatures (e.g., 1250 °C) is accelerated by factors of 9 and 23 by mechanical activation of silicon in either N_2 or NH_3. This has been attributed to the enhanced reactivity of Si and the entrapment of N_2 by mechanical activation [144].

Nanocomposite compositions consisting of titanium nitride and titanium diboride of particle sizes in the range of 5 to 10 nm were obtained by mechanical activation of Ti together with BN [145]. Similarly, AlN–TiB_2 nanocomposites can be fabricated by mechanical activation of Ti and Al together with BN, followed by sintering or hot pressing in order to densify the nanocomposites [146]. A nanocrystalline mixture of WC and intermediate tungsten carbide phases was generated by mechanical activation of WO_3 together with Mg and graphite, where the mechanochemical reaction took place in two steps [147], namely, formation of α-W as a result of explosive reduction of WO_3 by Mg and then the diffusion reaction between α-W and C. The product therefore consists of WC nanoparticles of 4 to 20 nm in size dispersed in MgO matrix, which can be washed off using HCl solution. Prolonged mechanical activation of rutile (TiO_2) together with aluminum in nitrogen produced a composite consisting of nanocrystalline alumina and titanium nitride, which undergo growth in crystallite and particle sizes upon subsequent annealing at 1200 °C [148].

In addition to carbides, nitrides, borides, and nanocomposites consisting of one or more carbide, nitride, and boride phases, other nonoxide ceramics and their nanocomposites that have been synthesized by mechanical activation include sulphides, silicides, and phosphates [149–158]. For example, mechanical activation of Ni together with P, and Al together with P, can lead to formation of nanocrystalline Ni- and Al-phosphides [154]. Bi_2Se_3 and BiSe were synthesized by mechanical activation of Bi + Se mixtures in the molar ratio of 2:3 and 1:1, respectively [155]. Formation of ZnS is realized by mechanical activation of $ZnCl_2$ and CdS in $CaCl_2$, which acts as a dispersion agent in refining the particle and agglomerate sizes [156]. Similarly, nanocrystalline cadmium sulphide (quantum dots) can be obtained by the displacement reaction between $CdCl_2$ and Na_2S triggered by mechanical activation, giving rise to CdS and NaCl [157]. Zirconium silicides can be synthesized by a mechanically induced self-propagating reaction, which is analogous to the thermally ignited self-propagating syntheses, where the explosive formation of zirconium silicides is attributed to the relatively large heat of formation involved [158].

6. MECHANICAL CRYSTALLIZATION AND PRECURSOR TO CERAMIC CONVERSIONS

High sintered density and uniform microstructure/nanostructure are among the most desirable features for almost all ceramic materials, as far as most of the functional and structural applications are concerned. Synthesis of a fine and sinterable ceramic powder is the first and perhaps the most important step in realization of a high sintered density and desirable microstructure/nanostructure at lowered sintering temperatures. Phase formation by a conventional ceramic fabrication technique (i.e., solid-state reaction of constituent oxides/nonoxides at elevated temperatures) is unable to deliver a fine and sinter-reactive ceramic powder, due to the unavoidable particle coarsening and aggregation at the calcination temperature, in combination with several other apparent detrimental effects such as nonstoichiometry and occurrence of impurity phases. This explains why for the past two decades considerable research efforts have been directed towards synthesis of nanocrystalline ceramic powders via a number of chemistry-based routes. Unfortunately, as mentioned earlier, almost all ceramic precursors derived from wet-chemistry routes have to be calcined at a temperature in the range of 500 to 1000 °C, in order to materialize the precursor to ceramic convention. Calcination of a ceramic precursor at an intermediate temperature ruins almost all the advantages offered by chemistry-based novel synthesis techniques, as a consequence of the particle coarsening and aggregation in the calcined ceramic powders. In this context, there is no fundamental difference between conventional ceramic and chemistry-based processing routes, where the problems are caused by the unavoidable calcination at high temperatures. Therefore, realization of the precursor to ceramic convention via an alternative, low temperature route represents a major advance in ceramic processing.

Mechanical crystallization in Fe-based amorphous alloys at room temperature was extensively studied following the pioneering work of Trudeau and Schulz [39], who demonstrated that nanocrystalline metallic phases of crystallite size in the range of 2 to 5 nm were triggered to form in certain amorphous alloy compositions by an input of mechanical energy [40]. The feasibility of mechanical crystallization in ceramic composition and the precursor to ceramic conversion by mechanical activation have been successfully demonstrated with an amorphous hydroxide precursor of PZT prepared via a co-precipitation route [159]. Figure 7 shows the XRD traces of the co-precipitated hydroxide precursor upon mechanical activation for 5, 15, and 35 hours, respectively, together with that of the amorphous precursor that was not subjected to any mechanical activation. Only one strong and broadened peak is observed over the 2θ angle of 28 to 35° for the starting hydroxide precursor, indicating its amorphous nature. Five hours of mechanical activation apparently led to a steady formation of PZT nanocrystallites in an essentially amorphous PZT precursor, while the transitional PT and PZ phases were not observed prior to formation of perovskite PZT phase. The intensity and sharpness of perovskite PZT (110), (100), (111), (200), (210), (211), and

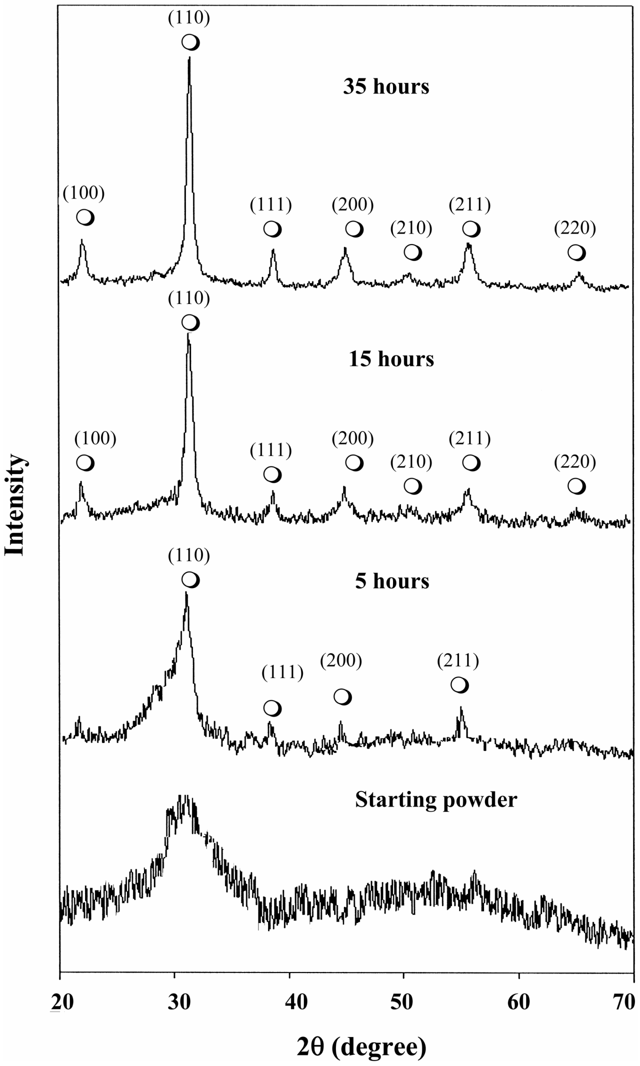

Figure 7. XRD traces of PZT precursor derived from co-precipitation when mechanically activated for various times ranging from 0 to 35 hours (❍: PZT). Reprinted with permission from [159], J. M. Xue et al., *J. Amer. Ceram. Soc.* 82, 1641 (1999). © 1999, American Ceramic Society.

(220) peaks were further established when the mechanical activation was extend to 15 and then 35 hours.

Mechanical activation has also been successfully applied to the precursor to ceramic transition in several other oxide ceramic systems, including α-Fe_2O_3, ZnO, CeO_2, Al_2O_3, and oxides ferrites. In general, oxide particles of nanocrystallinity and a minimized degree of particle aggregation are obtained, although the phase-forming mechanisms involved varied considerably from one material system to another. For example, formation of γ-Fe_2O_3 nanocrystallites triggered by mechanical activation, in an amorphous silica matrix from a sol–gel-derived precursor at room temperature, occurred by involving Fe_3O_4 as a transitional phase. Prolonged mechanical activation led to a steady phase transformation from Fe_3O_4 to γ-Fe_2O_3, as confirmed by phase identification and measurement in magnetic behavior [118].

Mechanical crystallization in oxide glass has recently been demonstrated by Xue and Wang [160], who employed two slightly different $PbNb_2O_6$ glass samples, which were quenched from 1300 and 1350 °C, respectively, for experimentation. As a result of the much higher glass-forming ability of the oxide glass than that of a metallic glass, it is much more difficult to induce crystallization in the former than that in the latter. Nevertheless, mechanical crystallization was observed in the glass quenched from 1300 °C, where a density of $PbNb_2O_6$ nuclei existed prior to mechanical activation. Mechanical activation promoted a steady growth in nanocrystallites of $PbNb_2O_6$, up to 15 nm in size. Due to the lack of $PbNb_2O_6$ nuclei in the glass quenched from 1350 °C, mechanical crystallization was not initiated by mechanical activation. This has led the investigators to believe that the mechanical crystallization in $PbNb_2O_6$ glass is nucleation-controlled. Although nucleation is thermodynamically favored at a low temperature, the inability of mechanical activation in triggering nucleation in the highly amorphous oxide glass is apparently due to its higher structural stability, as compared to that of Fe–Si–B based metallic glass.

7. SUMMARY

As a newly developed synthesis technique for nanocrystalline ceramic materials, mechanical activation can deliver the designed ceramic phase(s) and structure(s) by a single step of mechanical activation conducted in an enclosed activation chamber at room temperature. By employing the widely available oxides and nonoxides as the starting materials and skipping the multiple steps of phase formation at elevated temperatures that are always required in conventional solid state reaction, mechanical activation offers a lower manufacturing cost and a higher production yield, when compared to wet-chemistry-based synthesis techniques for ceramic materials. More importantly, mechanical activation delivers the much wanted nanocrystalline structures that cannot possibly be realized by either conventional ceramic processing or wet-chemistry-based synthesis techniques. In addition, a number of nanocrystalline ceramic materials derived from mechanical activation demonstrate unique structural metastability, extended solid solubility, and surface and structural defects (such as cation inversion in the spinel structures and order–disorder transitions in complex perovskites), which give rise to a number of unique electrical, electronic, magnetic, and functional properties.

On the one hand, phase formation processes triggered by mechanical activation are fundamentally different from those in the conventional solid-state reaction in many ceramic systems studied to date; mechanical activation can be used to synthesize ceramic materials that cannot possibly synthesized by either conventional ceramic processing or wet-chemistry-based techniques. Nanocrystalline PZN of complex perovskite structure is one such good example [89, 90]. On the other hand, a number of solid-state phenomena that are traditionally triggered by thermal activation can be made to take place by mechanical activation, including phase transition, order–disorder transformation in complex perovskite structure, and precursor to ceramic phase conversions, which are traditionally realized by calcination at elevated temperatures.

Mechanical activation has been successfully utilized to synthesize a wide range of nanocrystalline ceramic materials, including ceramic oxides, oxides of complex perovskite, spinel and layered perovskite structures, ceramic ferrites, nonoxide ceramics, and their nanocomposites. While phase formation triggered by mechanical activation is different from that in the conventional solid-state reaction, understanding the exact phase formation mechanisms in some of these nanocrystalline ceramic materials will apparently be one of the future developments in the study of mechanical activation. There are several unique phenomena that have been observed in association with mechanical activation, including the occurrence of metastable structures, order–disorder transformation in complex perovskites, and cation inversion in spinel structures. Both short-range and long-range structural disordering can be induced in certain Pb-based complex perovskites, for example in $Pb(Sc_{1/2}Ta_{1/2})O_3$, $Pb(Mg_{1/3}Nb_{2/3})$–$Pb(Mg_{1/2}W_{1/2})O_3$, by mechanical activation [38, 161]. There exists an equilibrium between mechanical activation and thermal activation in leading to the order–disorder transition in these perovskite structures, where mechanical activation induces disorder while thermal activation tends to recover the structural ordering. It will be considerably interesting to understand the exact physical principles behind these unique phenomena, as triggered by mechanical activation.

In order to further tailor the characteristics of nanocrystalline ceramic materials, mechanical activation can be combined with one or more other types of processing control. For example, mechanical activation can be assisted by an electrical discharge, magnetic field, hydrothermal conditions, and an effective integration of mechanical and thermal activations [11, 13, 14]. There is no doubt that this will also be one of the interesting areas for further development of mechanical activation.

Success of mechanical activation in synthesis of nanocrystalline ceramic material promises a significant technological implication, whereby the currently employed multiple steps of phase-forming calcination/annealing at high temperatures for ceramic materials can be skipped, when designed ceramic phases and chemical stoichiometry are realized at room temperature in an enclosed mechanical activation chamber. The scale-up of this novel synthesis technique to industrially useful batches will be technologically demanding and also a challenge in the future development of mechanical activation.

GLOSSARY

Complex ceramic oxide Those oxides containing more than one type of cation in structure, including those of perovskite structure, complex perovskite structure, aurivillius type compound and layered perovskite structure, spinel structure, and their solid solutions.

Mechanical activation A mechanical process, typically involving one or more processes of mechanical impact, shear, straining, deformation, mixing, and fracture at room temperature, above or below room temperature, that can activate the phenomena such as phase transformation, order-disorder transformation, structure change, surface modification, and in particular, formation of a new material phase as a result of the nucleation and crystallization triggered by such mechanical process. High energy mills are widely employed for mechanical activation.

Mechanical amorphization/crystallization Amorphization/crystallization triggered by a mechanical activation process.

Mechanochemical synthesis Materials synthesis involves one or more types of chemical processes/reactions triggered by a mechanical process, with or without the need for subsequent thermal annealing at elevated temperatures, in order to form the designed material phase/structure.

Nanocrystalline ceramics Those ceramic materials with microstructural feature in the nanometer scales, typically in the range of 1.0 to 100 nm.

Simple ceramic oxide Those oxides containing one predominant cation in structure, regardless of the structure types, with or without the involvement of other cations at a tracing level added as dopants. Typical examples of simple ceramic oxides are ZrO_2, CeO_2, ZnO and Al_2O_3.

ACKNOWLEDGMENTS

The authors acknowledge the input of and discussions with Wan Dongmei, Ng Wei Beng, Ang Seok Khim, Ng Sze Hwee, Gan Xingsen, Lim Hua Wei, and Liu Xiangyuan. Financial support by the National University of Singapore, the Institute of Materials Research and Engineering (IMRE, Singapore), and A*Star (Singapore) are acknowledged.

REFERENCES

1. P. G. McCormick and F. H. Froes, *JOM* 11, 61 (1998).
2. V. V. Boldyrev and K. Tkacova, *J. Mater. Synth. Process.* 8, 121 (2000).
3. J. S. Benjamin, *Sci. Amer.* 234, 40 (1976).
4. C. Suryanarayana, *Progr. Mater. Sci.* 46, 1 (2001).
5. E. Gaffet and O. Tillement, *Ann. Chim. Sci. Mater.* 22, 417 (1997).
6. E. Gaffet, F. Bernard, J. C. Niepce, F. Charlot, C. H. Gras, G. Le Caer, J. L. Guichard, P. Delcroix, A. Mocellin, and O. Tillement, *J. Mater. Chem.* 9, 305 (1999).
7. A. Calka, *Appl. Phys. Lett.* 59, 1568 (1991).
8. M. S. El-Eskandarany, K. Aoki, and K. Suzuki, *J. Less-Common Metals* 167, 113 (1990).
9. V. Gauthier, C. Josse, F. Bernard, E. Gaffet, and J. P. Larpin, *Mater. Sci. Eng. A* 265, 117 (1999).
10. C. H. Gras, F. Charlot, E. Gaffet, F. Bernard, and J. C. Niepce, *Acta Mater.* 47, 2113 (1999).
11. L. L. Shaw, *Mater. Manuf. Process.* 16, 405 (2001).
12. L. L. Shaw, *Adv. Eng. Mater.* 2, 721 (2000).
13. R. M. Ren, Z. G. Yang, and L. L. Shaw, *J. Amer. Ceram. Soc.* 85, 819 (2002).
14. A. Calka and D. Wexler, *Nature* 419, 147 (2002).
15. K. Niihara and A. Nakahira, *Ann. Chim. Sci. Mater.* 16, 479 (1991).
16. B. N. Kim, K. Hiraga, K. Morita, and Y. Sakka, *Nature* 413, 288 (2001).
17. F. Wakai, N. Kondo, and Y. Shinoda, *Current Opinion Solid State Mater. Sci.* 4, 461 (1999).
18. E. J. W. Verwey and E. L. Hailmann, *J. Chem. Phys.* 15, 174 (1947).
19. W. D. Kingery, H. K. Bowen, and D. R. Uhlmann, in "Introduction to Ceramics," p. 991. Wiley, New York (1976).

20. K. Tanaka, M. Makita, Y. Shimizugawa, K. Hirao, and N. Soga, *J. Phys. Chem. Solids* 59, 1611 (1998).
21. G. F. Goya and H. R. Rechenberg, *J. Magn. Magn. Mater.* 196–197, 191 (1999).
22. T. M. Clark and B. J. Evans, *IEEE Trans. Magn.* 33, 3745 (1997).
23. J. F. Hochepied, P. Bonville, and M. P. Pileni, *J. Phys. Chem. B* 104, 905 (2000).
24. T. Sato, K. Haneda, T. Iijima, and M. Seki, in "Proceedings of the Sixth International Conference on Ferrites (ICF6)," Tokyo and Kyoto, Japan, p. 984, 1992.
25. T. Kamiyama, K. Haneda, T. Sato, S. Ikeda, and H. Asano, *Solid State Comm.* 81, 563 (1992).
26. Z. H. Zhou, J. M. Xue, J. Wang, H. S. O. Chan, T. Yu, and Z. X. Shen, *J. Appl. Phys.* 91, 6015 (2002).
27. O. Furukawa, M. Harata, Y. Yamashita, K. Inagaki, and S. Mukaeda, *Jpn. J. Appl. Phys.* 26, 34 (1987).
28. L. F. Francis, Y. J. Oh, and D. A. Payne, *J. Mater. Sci.* 25, 5007 (1990).
29. K. S. Mazdiyasni and L. M. Brown, *J. Amer. Ceram. Soc.* 55, 633 (1972).
30. T. R. N. Kutty and R. Balachandran, *Mater. Res. Bull.* 19, 1497 (1984).
31. J. H. Choy, Y. S. Han, and J. T. Kim, *J. Mater. Chem.* 5, 65 (1995).
32. J. M. Xue, D. M. Wan, S. E. Lee, and J. Wang, *J. Amer. Ceram. Soc.* 82, 1687 (1999).
33. B. L. Huang, R. J. Perez, E. J. Lavernia, and M. J. Luton, *Nanostruct. Mater.* 7, 67 (1996).
34. K. Chattopadhyay, X. M. Wang, K. Aoki, and T. Masumoto, *J. Alloys Compds.* 232, 224 (1996).
35. H. J. Fecht, *Nature* 356, 133 (1992).
36. B. Bokhonov, I. Konstanchuk, E. Ivanov, and V. Boldyrev, *J. Alloys Compds.* 187, 207 (1992).
37. B. Bokhonov, I. Konstanchuk, and V. Boldyrev, *J. Non-Cryst. Solids* 153–154, 606 (1993).
38. X. S. Gao, J. M. Xue, T. Yu, Z. X. Shen, and J. Wang, *J. Amer. Ceram. Soc.* 85, 833 (2002).
39. M. L. Trudeau and R. Schulz, *Phys. Rev. Lett.* 64, 99 (1990).
40. H. Chen, Y. He, G. J. Shiflet, and S. J. Poon, *Nature* 367, 541 (1994).
41. J. J. Gilman, *Science* 274, 65 (1996).
42. P. G. McCormick, T. Tsuzuki, J. S. Robinson, and J. Ding, *Adv. Mater.* 13, 1008 (2001).
43. J. Ding, T. Tsuzuki, P. G. McCormick, and R. Street, *J. Alloys Compds.* 234, L1 (1996).
44. G. Garcia-Pacheco, J. G. Cabanas-Moreno, F. Cruz-Gandarilla, H. Yee-Madeira, and M. Umemoto, *Mater. Sci. Forum* 386, 281 (2002).
45. H. Yang, G. Nguyeb, and P. G. McCormick, *Scripta Metall. Mater.* 32, 681 (1995).
46. V. V. Blaskov, D. D. Radev, D. Klissurski, and N. D. Yordanov, *J. Alloys Compds.* 206, 267 (1994).
47. T. Watanabe, T. Isobe, and M. Senna, *J. Solid State Chem.* 122, 74 (1996).
48. J. Wang, J. M. Xue, D. M. Wan, and B. K. Gan, *J. Solid State Chem.* 154, 321 (2000).
49. M. Senna, *Int. J. Inor. Mater.* 3, 509 (2001).
50. V. V. Boldyrev, *Powder Tech.* 122, 247 (2002).
51. J. Ding, T. Tsuzuki, and P. G. McCormick, *J. Amer. Ceram. Soc.* 79, 2956 (1996).
52. J. Ding, T. Tsuzuki, and P. G. McCormick, *Nanostruct. Mater.* 8, 75 (1997).
53. A. C. Dodd and P. G. McCormick, *J. Euro. Ceram. Soc.* 22, 1823 (2002).
54. P. N. Kuznetsov, L. I. Kuznetsova, A. M. Zhyzhaev, G. L. Pashkov, and V. V. Boldyrev, *Appl. Catal. A* 227, 229 (2002).
55. J. Ding, T. Tsuzuki, and P. G. McCormick, *Nanostruct. Mater.* 8, 739 (1997).
56. T. Tsuzuki, E. Pirault, and P. G. McCormick, *Nanostruct. Mater.* 11, 125 (1999).
57. T. Tsuzuki and P. G. McCormick, *J. Amer. Ceram. Soc.* 84, 1453 (2001).
58. U. Kerson, *Appl. Phys. A* 75, 559 (2002).
59. T. Tsuzuki and P. G. McCormick, *Mater. Sci. Forum* 343, 383 (2000).
60. P. G. McCormick and T. Tsuzuki, *Mater. Sci. Forum* 386, 377 (2002).
61. Y. Chen and J. S. Williams, *Mater. Sci. Forum* 235, 985 (1997).
62. P. N. Kutnesov, L. I. Kuznetsova, A. M. Zhizhaev, S. M. Kolesnikova, G. L. Pashkov, and V. V. Boldyrev, *Russ. J. Inor. Chem.* 47, 393 (2002).
63. P. F. Chong, J. M. Xue, and J. Wang, *J. Amer. Ceram. Soc.* 85, 273 (2002).
64. J. Subrt, V. Balek, J. M. Criado, L. A. Perez-Maqueda, and E. Vecernikova, *J. Therm. Anal. Calorim.* 53, 509 (1998).
65. T. Puclin, W. A. Kaczmarek, and B. W. Ninham, *Mater. Chem. Phys.* 40, 73 (1995).
66. K. A. Evans, *Key Eng. Mater.* 122, 489 (1996).
67. A. Tonejc, A. M. Tonejc, D. Bagovic, and C. Kosanovic, *Mater. Sci. Eng. A* 182, 1227 (1994).
68. C. C. Yong and J. Wang, *J. Amer. Ceram. Soc.* 84, 1225 (2001).
69. P. M. Botta, P. G. Beroff, E. F. Ahlietti, H. R. Bertorello, and J. M. P. Lopez, *J. Mater. Sci.* 37, 2563 (2002).
70. Y. Chen and J. S. Williams, *J. Mater. Res.* 13, 3499 (1998).
71. N. J. Welham, *J. Alloys Compds.* 274, 303 (1998).
72. N. J. Welham, *J. Alloys Compds.* 270, 228 (1998).
73. P. P. Pradeep and H. R. Subhash, *J. Mater. Sci.* 25, 1169 (1990).
74. J. M. Xue, J. Wang, and D.M. Wan, *J. Amer. Ceram. Soc.* 83, 232 (2000).
75. O. Abe and Y. Suzuki, *Mater. Sci. Forum* 225, 563 (1996).
76. N. J. Welham, *J. Mater. Res.* 13, 1607 (1998).
77. J. G. Baek, T. Isobe, and M. Senna, *Solid State Ionics* 90, 269 (1996).
78. D. Durovic, E. Kostic, S. J. Kiss, and S. Zec, *J. Alloys Compds.* 279, L1 (1998).
79. V. V. Zyryanov, *Inor. Mater.* 35, 935 (1999).
80. K. Hamada and M. Senna, *J. Mater. Sci.* 31, 1725 (1996).
81. J. M. Xue, D. M. Wan, and J. Wang, *Solid State Ionics* 151, 403 (2002).
82. S. L. Swartz, T. R. Shrout, W. A. Schulze, and L. E. Cross, *J. Amer. Ceram. Soc.* 67, 311 (1984).
83. S. L. Swartz and T. R. Shrout, *Mater. Res. Bull.* 17, 1245 (1982).
84. T. R. Shrout and A. Halliyal, *Amer. Ceram. Soc. Bull.* 66, 704 (1987).
85. J. Wang, J. M. Xue, D. M. Wan, and W. B. Ng, *Solid State Ionics* 124, 271 (1999).
86. H. P. Klug and L. E. Alexander, "X-ray Diffraction Procedures for Polycrystalline and Amorphous Materials," pp. 491–538. Wiley, New York, 1954.
87. A. N. Dremin and O. N. Breusov, *Russ. Chem. Rev.* 37, 392 (1968).
88. N. N. Thadhani, *J. Appl. Phys.* 76, 2129 (1994).
89. D. M. Wan, J. M. Xue, and J. Wang, *J. Amer. Ceram. Soc.* 83, 53 (2000).
90. J. Wang, D. M. Wan, J. M. Xue, and W. B. Ng, *J. Amer. Ceram. Soc.* 82, 477 (1999).
91. Y. Noguchi, I. Miwa, Y. Goshima, and M. Miyayama, *Jpn. J. Appl. Phys.* 39, L1259 (2000).
92. J. G. Lisoni, P. Millan, E. Vila, J. L. M. de Vidales, T. Hoffmann, and A. Castro, *Chem. Mater.* 13, 2084 (2001).
93. S. H. Ng, J. M. Xue, and J. Wang, *Mater. Chem. Phys.* 75, 131 (2002).
94. M. H. Sim, J. M. Xue, and J. Wang, submitted for publication.
95. Q. W. Zhang, T. Nakagawa, and F. Saito, *J. Alloys Compds.* 308, 121 (2000).
96. Q. W. Zhang and T. Saito, *J. Alloys Compds.* 297, 99 (2000).

97. R. Uribe, C. Baudi, L. Mazerolles, and D. Michel, *J. Mater. Sci.* 36, 5105 (2001).
98. L. B. Kong, J. Ma, and H. Huang, *J. Alloys Compds.* 336, 315 (2002).
99. A. Castro, P. Millan, L. Pardo, and B. Jimenez, *J. Mater. Chem.* 9, 1313 (1999).
100. Q. W. Zhang, and F. Saito, *J. Mater. Sci.* 36, 2287 (2001).
101. W. T. Jeong and K. S. Lee, *J. Power Sources* 104, 195 (2002).
102. Y. Okamoto, T. Isobe, and M. Senna, *J. Non-Cryst. Solids* 180, 171 (1995).
103. N. V. Kosova, E. T. Devyatkina, and S. G. Kozlova, *J. Power Sources* 97, 406 (2001).
104. K. J. D. Mackenzie, J. Temuujin, T. Jadambaa, M. E. Smith, and P. Angerer, *J. Mater. Sci.* 35, 5529 (2000).
105. G. M. Mi, Y. Murakami, D. Shindo, and F. Saito, *Powder Tech.* 105, 162 (1999).
106. T. Hungria, J. G. Lisoni, and A. Castro, *Chem. Mater.* 14, 1747 (2002).
107. Q. W. Zhang, J. F. Lu, and F. Saito, *Powder Tech.* 122, 145 (2002).
108. L. Pardo, A. Castro, P. Millan, C. Alemany, R. Jimenez, and B. Jimenez, *Acta Mater.* 48, 2421 (2000).
109. J. Ricote, L. Pardo, A. Castro, and P. Millan, *J. Solid State Chem.* 160, 54 (2001).
110. A. Castro and D. Palem, *J. Mater. Chem.* 12, 2774 (2002).
111. J. F. Liao and M. Senna, *Mater. Res. Bull.* 30, 385 (1995).
112. J. Temuujin, K. Okada, and K. J. D. MacKenzie, *J. Euro. Ceram. Soc.* 18, 831 (1998).
113. J. Temuujin, K. Okada, and K. J. D. MacKenzie, *J. Solid State Chem.* 138, 169 (1998).
114. F. Saito, G. M. Mi, and M. Hanada, *Solid State Ionics* 101, 37 (1997).
115. I. Lapides, S. Yariv, N. Lahav, and I. Brodsky, *Colloid Polymer Sci.* 276, 601 (1998).
116. J. Ding, T. Tsuzuki, and P. G. McCormick, *Nanostruct. Mater.* 8, 739 (1997).
117. M. Zdujic, C. Jovalekic, L. Karanovic, M. Mitric, D. Poleti, and D. Skala, *Mater. Sci. Eng. A* 245, 109 (1998).
118. J. M. Xue, Z. H. Zhou, and J. Wang, *J. Amer. Ceram. Soc.* 85, 807 (2002).
119. C. N. Chinnasamy, A. Narayanasamy, N. Ponpandian, K. Chattopadhyay, H. Guerault, and J. M. Greneche, *J. Phys. Condens. Mater.* 12, 7795 (2000).
120. J. S. Jiang, X. L. Yang, L. Gao, J. K. Guo, and J. Z. Jiang, *Nanostruct. Mater.* 12, 143 (1999).
121. C. Jovalekic, M. Zdujic, A. Radakovic, and M. Mitric, *Mater. Lett.* 24, 365 (1995).
122. D. J. Fatemi, V. G. Harris, V. M. Browning, and J. P. Kirkland, *J. Appl. Phys.* 83, 6867 (1998).
123. J. S. Jiang, L. Gao, J. K. Guo, and X. L. Yang, *J. Inor. Mater.* 13, 415 (1998).
124. D. Arcos, N. Rangavittal, M. Vazquez, and M. Vallet-Regi, *Mater. Sci. Forum* 269, 87 (1998).
125. O. Abe and M. Narita, *Solid State Ionics* 101, 103 (1997).
126. J. Ding, T. Tsuzuki, and P. G. McCormick, *J. Magn. Magn. Mater.* 177, 931 (1998).
127. J. Ding, X. Y. Liu, J. Wang, and S. Yu, *Mater. Lett.* 44, 19 (2000).
128. M. Zdujic, C. Jovalekic, L. Karanovic, and M. Mitric, *Mater. Sci. Eng. A* 262, 204 (1999).
129. S. J. Campbell, W. A. Kaczmarek, and G. M. Wang, *Nanostruct. Mater.* 6, 735 (1995).
130. M. Hofmann, S. J. Campbell, and W. A. Kaczmarek, *Mater. Sci. Forum* 228, 607 (1996).
131. I. Mitov, Cherkezova, Z. Zheleva, and V. Mitrov, *Physica Status Solidi A* 161, 475 (1997).
132. M. Muroi, R. Street, P. G. McCormick, and J. Amighian, *Phys. Rev. B* 63, 184414 (2001).
133. H. H. Hamdeh, J. C. Ho, S. A. Oliver, R. J. Willey, G. Oliveri, and G. Busca, *J. Appl. Phys.* 81, 1851 (1997).
134. M. H. Mahmoud, H. H. Hamdeh, A. I. Abdel-Mageed, A. M. Abdallah, and M. K. Fayek, *Physica B* 291, 49 (2000).
135. V. Sepelak, A. Buchal, K. Tkacova, and K. D. Becker, *Mater. Sci. Forum* 278–281, 862 (1998).
136. V. Raul, "Magnetic Ceramics." Cambridge Univ. Press, Cambridge, UK, 1994.
137. B. Yao, S. E. Liu, L. Liu, L. Si, W. H. Su, and Y. Li, *J. Appl. Phys.* 90, 1650 (2001).
138. Y. HiBi and Y. Enomoto, *J. Mater. Sci. Lett.* 16, 316 (1997).
139. S. Horiuchi, J. Y. Huang, L. L. He, J. F. Mao, and T. Taniguchi, *Philos. Mag.* 78, 1065 (1998).
140. K. Kudaka, K. Iizumi, and T. Sasaki, *J. Ceram. Soc. Jpn.* 107, 1019 (1999).
141. A. A. Popovich, *Steel Transl.* 23, 56 (1993).
142. D. D. Radev and D. Klisurski, *J. Alloys Compds.* 206, 39 (1994).
143. F. J. Gotor, M. D. Alcala, C. Real, and J. M. Criado, *J. Mater. Res.* 17, 1655 (2002).
144. L. L. Shaw, Z. G. Yang, and R. M. Ren, *J. Amer. Ceram. Soc.* 81, 760 (1998).
145. J. L. Li, K. Hu, and Y. Zhong, *J. Mater. Sci. Tech.* 17, S101 (2001).
146. H. J. Kim, H. J. Choi, and J. G. Lee, *J. Amer. Ceram. Soc.* 85, 1022 (2002).
147. G. L. Tan and X. J. Wu, *Powder Metall.* 41, 300 (1998).
148. N. J. Welham, T. Kerr, and P. E. Willis, *J. Amer. Ceram. Soc.* 82, 2332 (1999).
149. G. V. Golubkova, E. Y. Belyaev, and O. I. Lomovsky, *J. Alloys Compds.* 270, 224 (1998).
150. J. H. Shim, J. S. Byun, and Y. W. Cho, *Scripta Mater.* 47, 493 (2002).
151. D. I. Kochubey, E. B. Burgina, R. Roy, and D. K. Agrawal, *J. Mater. Synth. Process.* 8, 279 (2000).
152. P. Balaz, L. Takacs, T. Ohtani, D. E. Mack, E. Boldizarova, V. Soika, and M. Achimovicova, *J. Alloys Compds.* 337, 76 (2002).
153. K. Kudaka, K. Iizumi, T. Sasaki, and H. Izumi, *J. Amer. Ceram. Soc.* 83, 2887 (2000).
154. L. Takacs and S. K. Mandal, *Mater. Sci. Eng. A* 304, 429 (2001).
155. E. Klose and R. Blachnik, *Thermochim. Acta* 375, 147 (2001).
156. T. Tsuzuki, J. Ding, and P. G. McCormick, *Physica B* 239, 378 (1997).
157. T. Tsuzuki and P. G. McCormick, *Appl. Phys. A* 65, 607 (1997).
158. B. K. Yen, *J. Alloys Compds.* 268, 266 (1998).
159. J. M. Xue, D. M. Wan, S. E. Lee, and J. Wang, *J. Amer. Ceram. Soc.* 82, 1641 (1999).
160. J. M. Xue and J. Wang, *J. Amer. Ceram. Soc.* 84, 2691 (2001).
161. X. S. Gao, J. Lim, J. M. Xue, J. S. Wang, and J. Wang, *J. Phys. Condens. Mater.* 14, 8639 (2002).